# Supporting Information

## High-Entropy Solvation Chemistry towards Affordable and Practical Ah-level Zinc Metal Battery

*Linhui Chang [1], Hongwei Cheng [1,*], Jiamin Li [1], Lei Zhang [2], Bomian Zhang [2], Liheng Zheng [2], Qiangchao Sun [1], Jiantao Li [3], Xionggang Lu [1,*], Kangning Zhao [4,*]*

[1] School of Materials Science and Engineering & State Key Laboratory of Advanced Special Steel, Shanghai University, Shanghai 200444, P. R. China.

[2] School of Materials Science and Engineering, Wuhan University of Technology, Wuhan 430070, P. R. China.

[3] Department of Chemical and Biological Engineering, Northwestern University, Evanston, IL 60208, USA

[4] School of Physical Sciences, Great Bay University, Dongguan, 523000 P. R. China.

* Email: hwcheng@shu.edu.cn; luxg@shu.edu.cn; vicyel@gbu.edu.cn

# Supplementary Figures and Tables

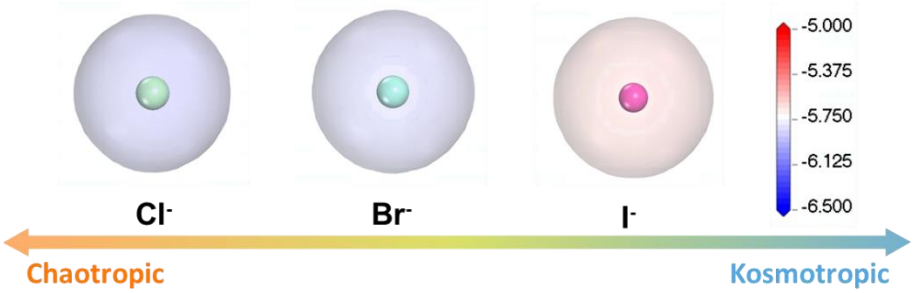


**Fig. S1** Properties of halogen ions, *Hofmeister* series

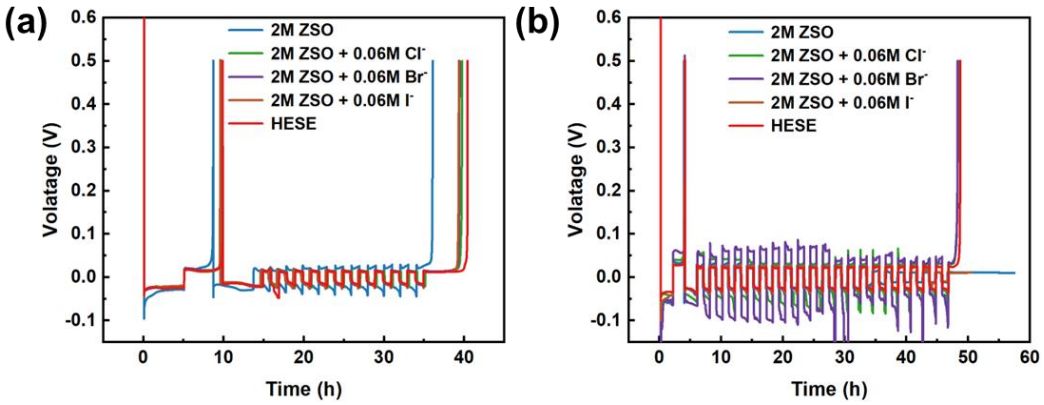


**Fig. S2** Coulombic efficiency of Zn||Cu asymmetric cell with different electrolytes by *Aurbach's* method under the conditions (a) (1 mA $cm^{-2}$, 5 mAh $cm^{-2}$)+( 1 mA $cm^{-2}$, 1 mAh $cm^{-2}$)*10, (b) (5 mA $cm^{-2}$, 10 mAh $cm^{-2}$)+(5 mA $cm^{-2}$, 5 mAh $cm^{-2}$)*20

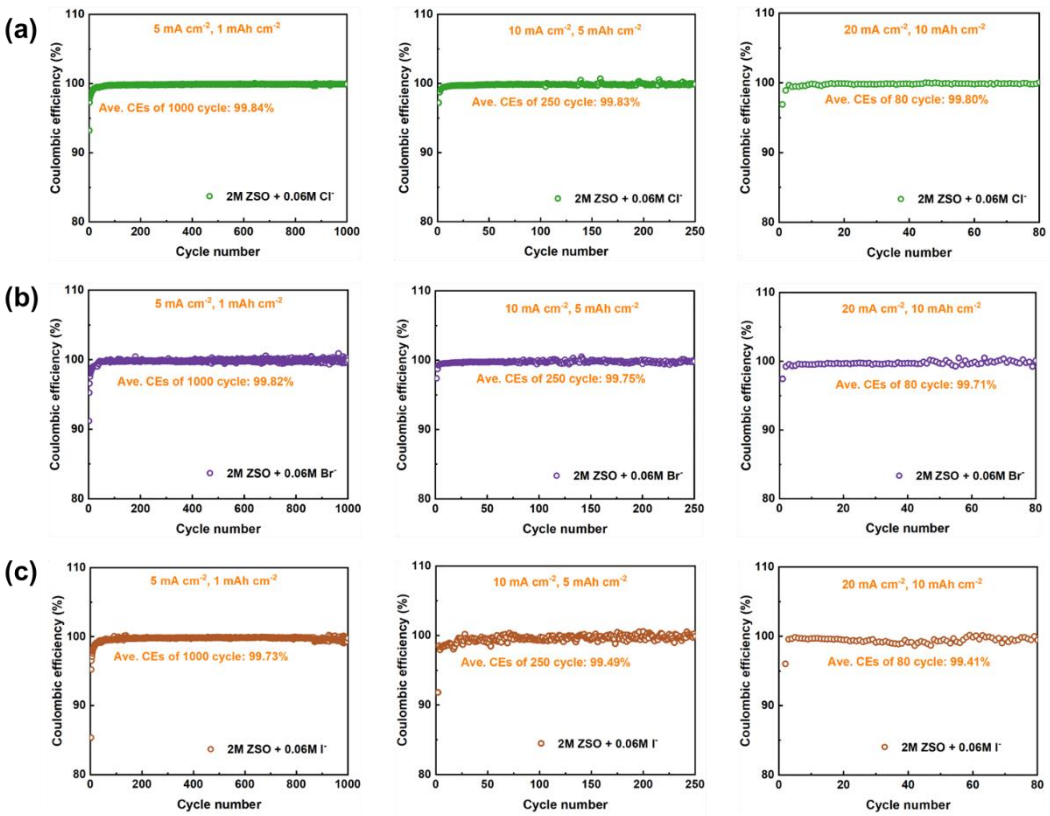


**Fig. S3** Coulombic efficiency of Zn||Cu asymmetric cells in electrolytes with single anion addition (a) 2M+0.06M $Cl^-$, (b) 2M+0.06M $Br^-$, and (c) 2M+0.06M $I^-$ electrolytes

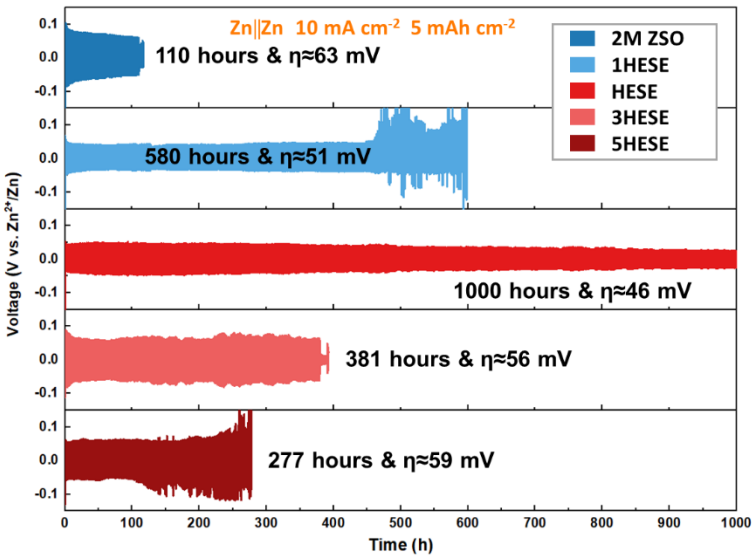


**Fig. S4** Long-cycle performance of Zn||Zn symmetric cells with different electrolytes at 10 mA $cm^{-2}$ and 5 mAh $cm^{-2}$

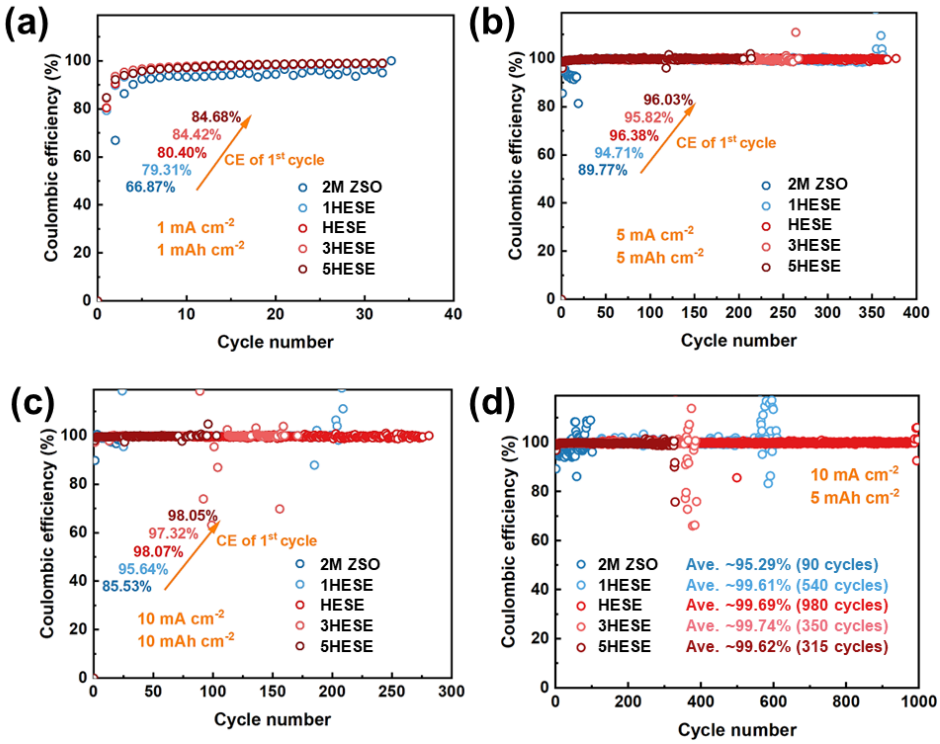


**Fig. S5** Average Coulombic efficiency of Zn||Cu asymmetric cells using different electrolytes at (a) 1 mA $cm^{-2}$, 1 mAh $cm^{-2}$, (b) 5 mA $cm^{-2}$, 5 mAh $cm^{-2}$, (c) 10 mA $cm^{-2}$, 10 mAh $cm^{-2}$, and (d) 10 mA $cm^{-2}$ and 5 mAh $cm^{-2}$

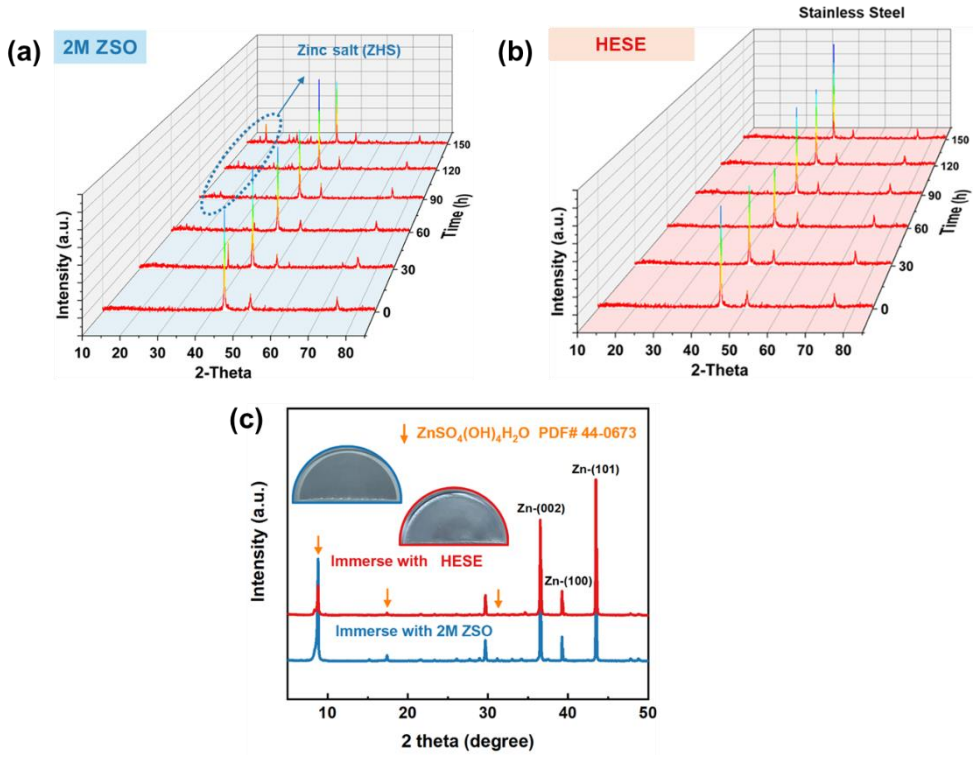


**Fig. S6** Ex-situ XRD of stainless steel collector in cells using (a) baseline electrolyte and (b) HESE. (c) XRD pattern of zinc metal after 5 days of immersion in two electrolytes (inset is the optical photograph)

**Supplementary Note 1**: The corrosiveness of halogen ions in solution is an important issue that cannot be ignored. XRD was used to detect the corrosion of the electrolyte on the stainless-steel collector and the surface by-products of zinc sheets, which demonstrated a slower corrosion rate of zinc in HESE and a significant inhibitory effect of HESE on by-products.

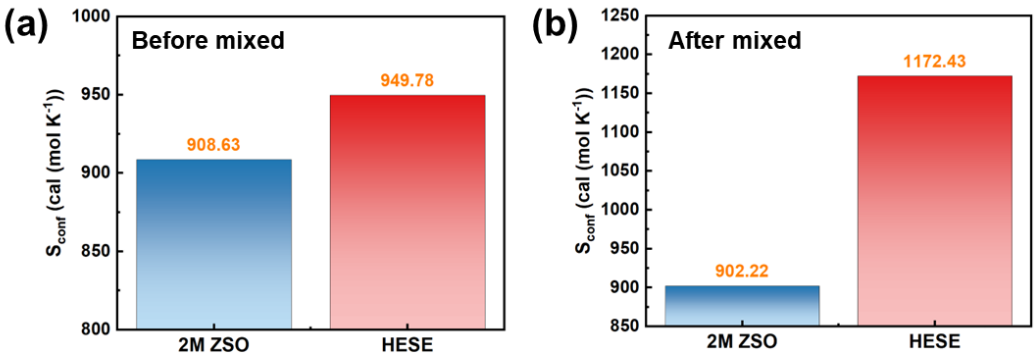


**Fig.S7** The calculated configurational entropy ($S_{conf}$) (a) before and (b) after mixed

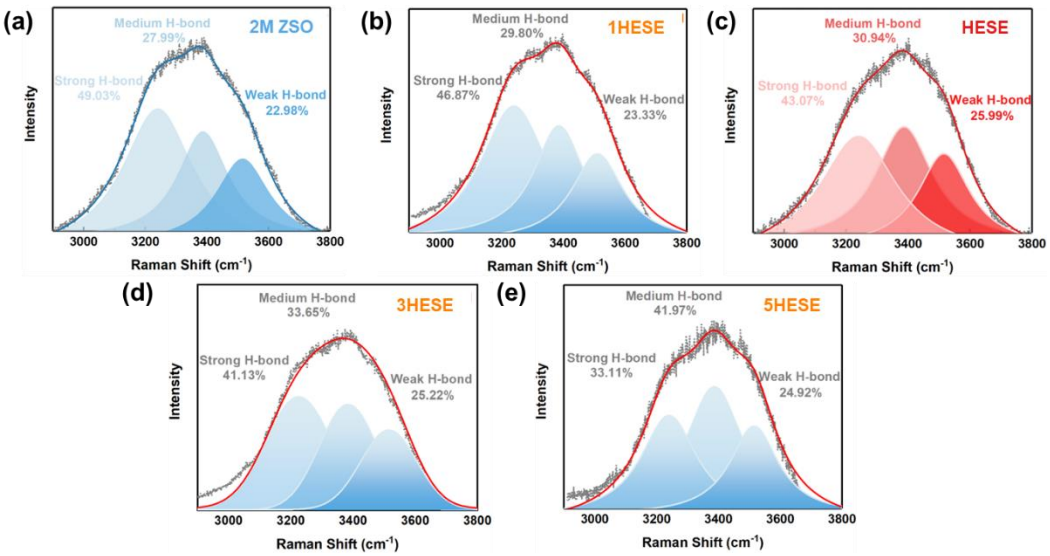


**Fig. S8** Raman spectra fitting results of *v*-O-H portion (strong, medium, and weak H-bonds) in (a) 2M ZSO, (b) 1HESE, (c) HESE, (d) 3HESE, and (e) 5HESE

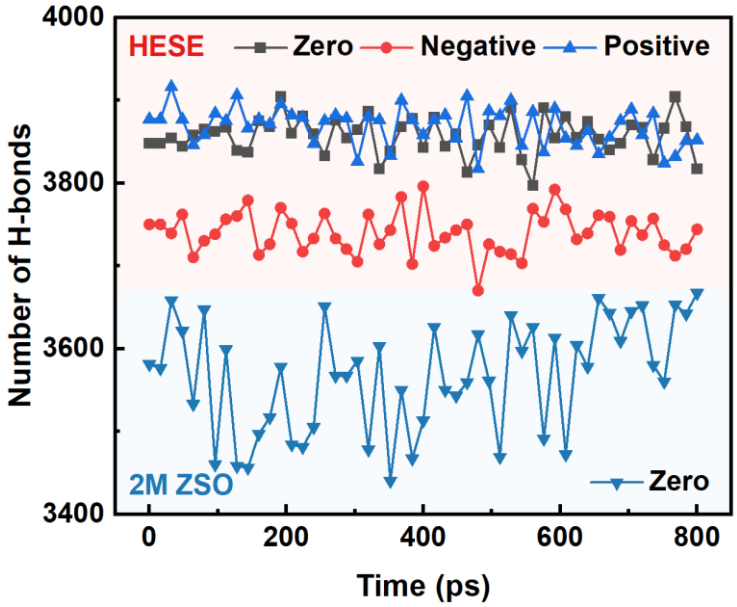


**Fig. S9** The lifetime and the numbers of H-bonds of HESE and 2M ZSO

**Supplementary Note 2:** This phenomenon might result from the intense bonding effects between halogen ions and water, which substantially elevates the number of hydrogen bond in HESE. The relatively stable number of hydrogen bonds in the zero-charge state may help the battery maintain stable performance during the cycling process and extend the service life. The increase in the number of hydrogen bonds in the negatively charged state may help to increase the rate of ion transport, thus improving the efficiency of the battery's charge and discharge. Increased hydrogen bonds in the positively charged state may enhance battery capacity.

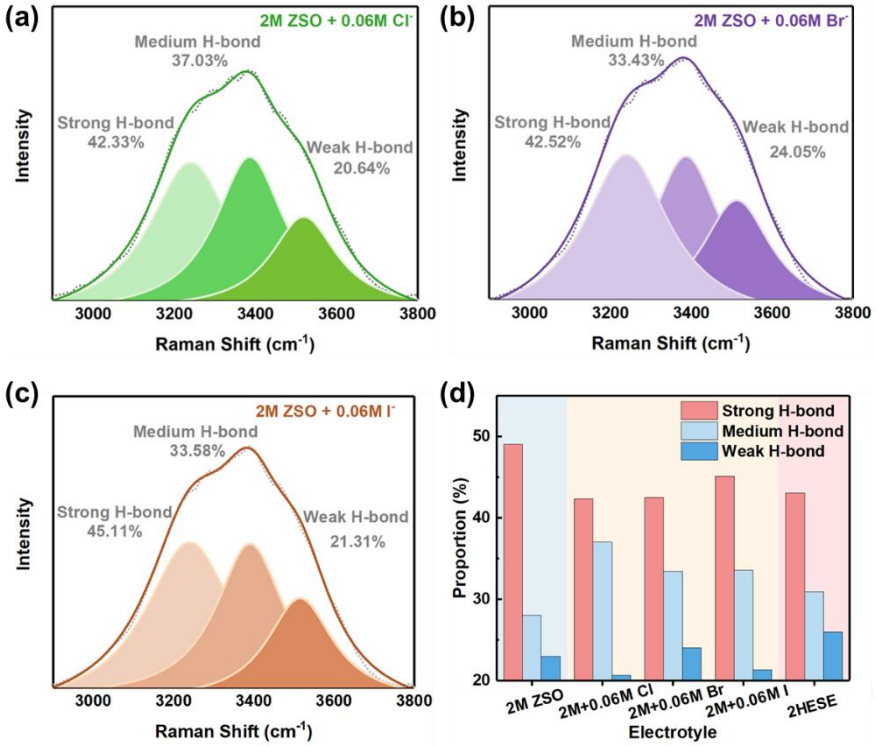


**Fig.S10** Raman spectra fitting results of *v*-O-H portion (strong, medium, and weak H-bonds) in (a) 2M+0.06M $Cl^-$, (b) 2M+0.06M $Br^-$, and (c) 2M+0.06M $I^-$ electrolyte, (d) Statistical results

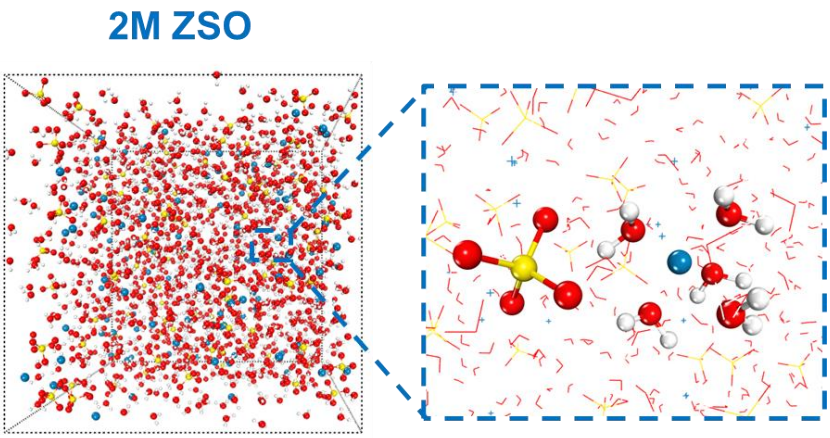


**Fig. S11** 3D snapshot and local amplification of MD simulations of 2M ZSO electrolyte system

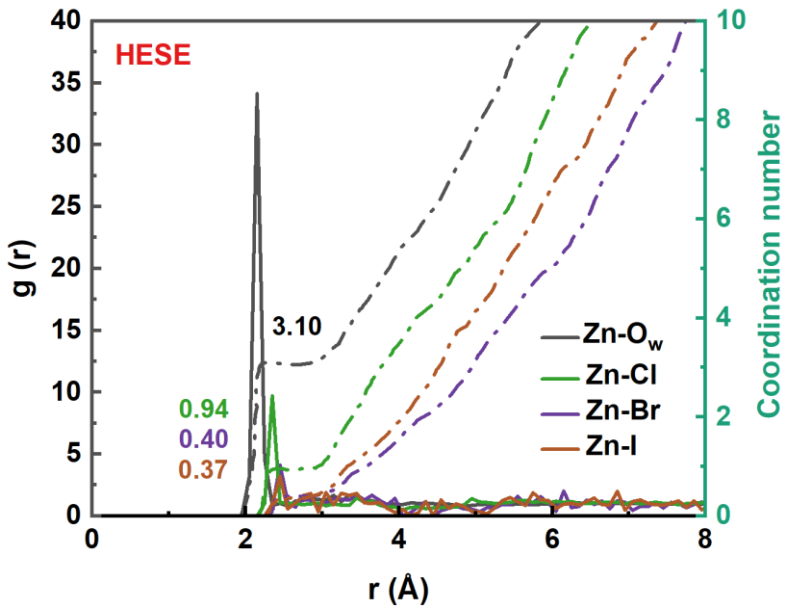


**Fig. S12** The coordination between Zn and each other atoms in HESE system

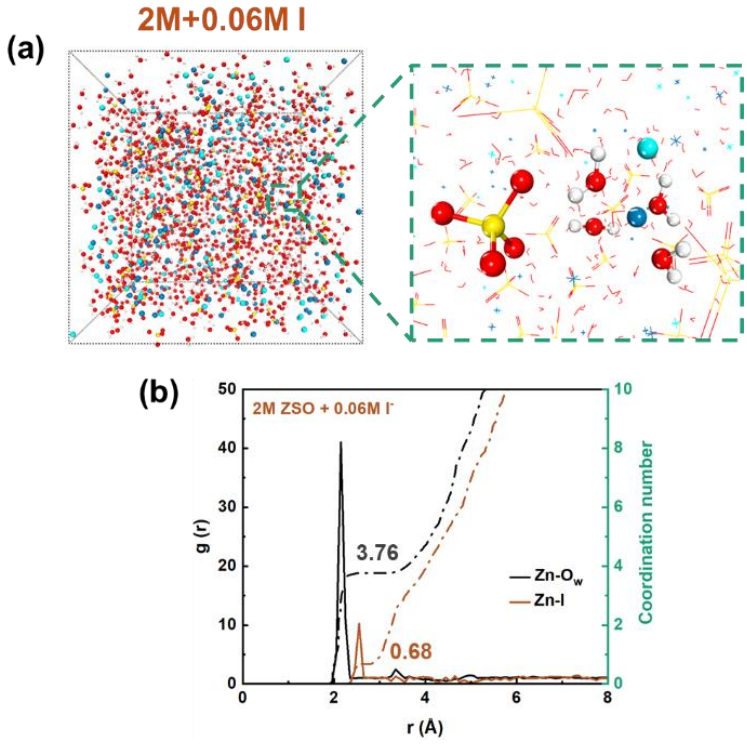


**Fig. S13** (a) 3D snapshot and local amplification, (b) The coordination between Zn and I of 2M+0.06M $I^-$ electrolyte system

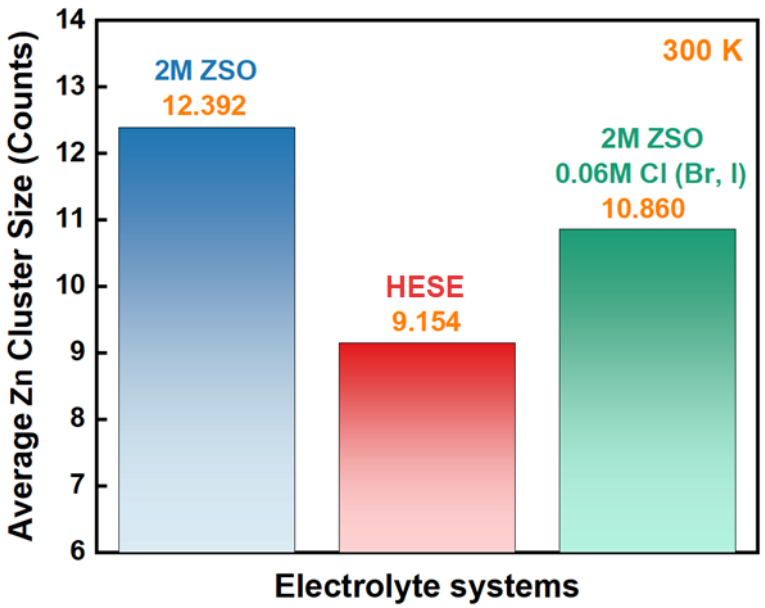


**Fig. S14** Average $Zn^{2+}$ cluster sizes in different electrolytes

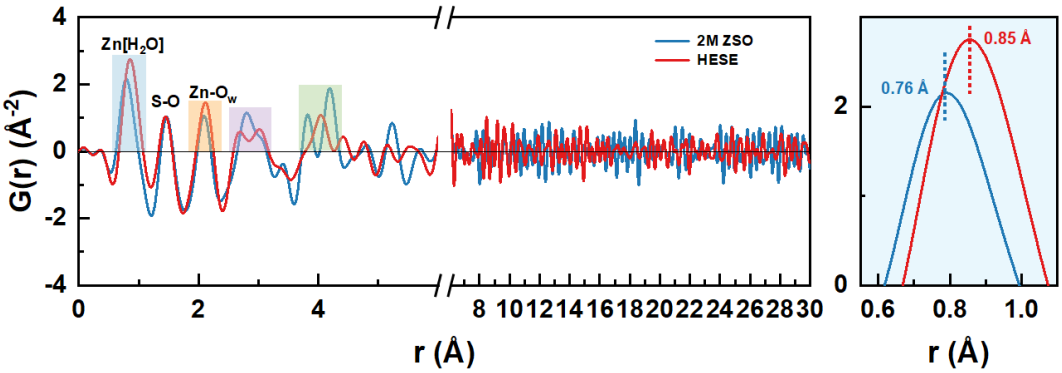


**Fig. S15** The pair distribution function (PDF) spectra of two electrolyte solutions

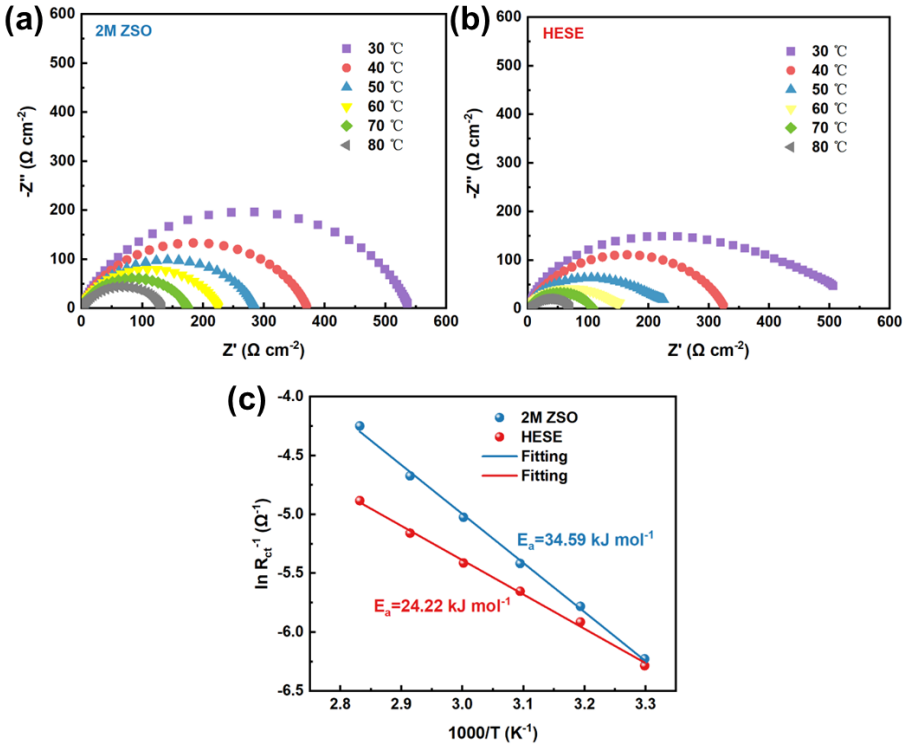


**Fig. S16** EIS curves of Zn||Zn symmetric cells at different temperatures in (a) 2M ZSO and (b) HESE, and (c) the calculated activation energy ($E_a$)

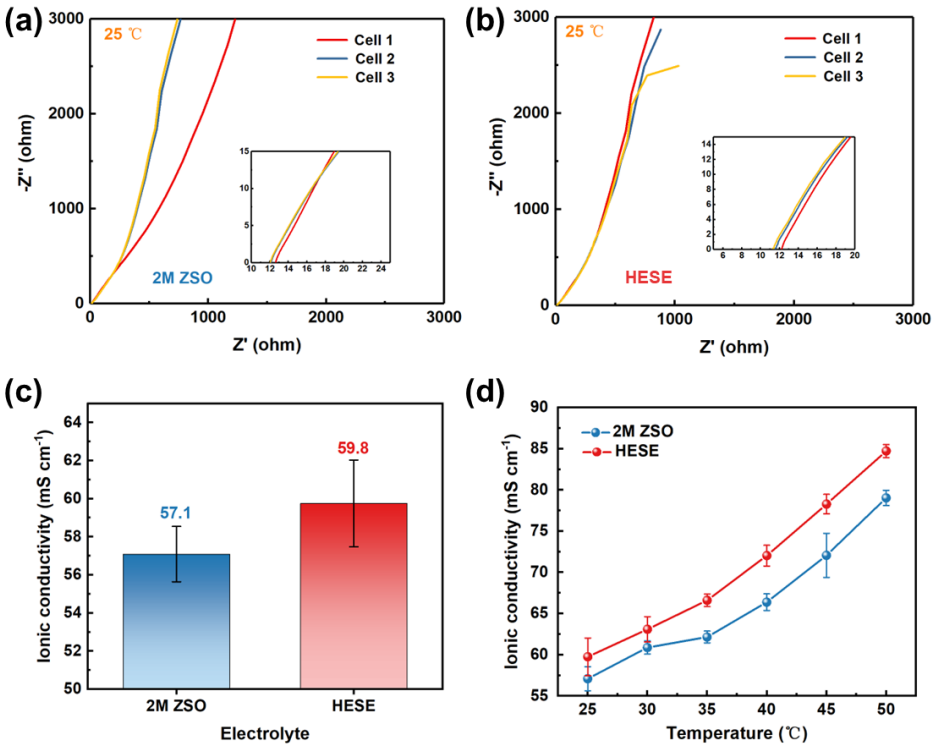


**Fig. S17** (a-b) EIS curves of two electrolytes at 25℃, Ionic conductivity at (c) 25℃ and (d) different temperatures

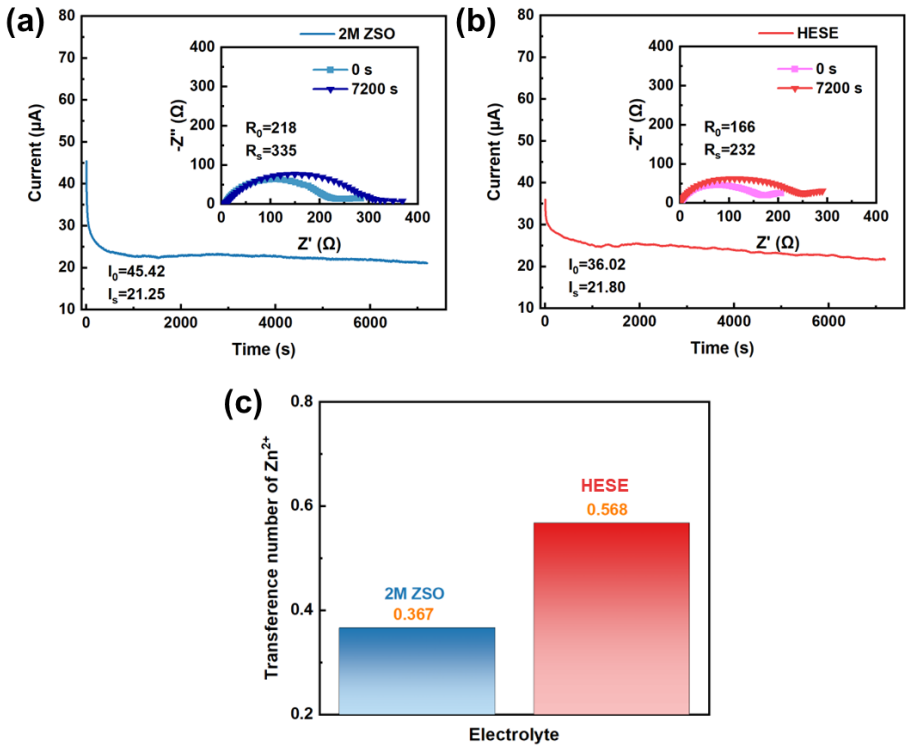


**Fig. S18** Chronoamperograms (CA) and EIS curves in (a) 2M ZSO and (b) HESE, (c) the calculated transference number of $Zn^{2+}$

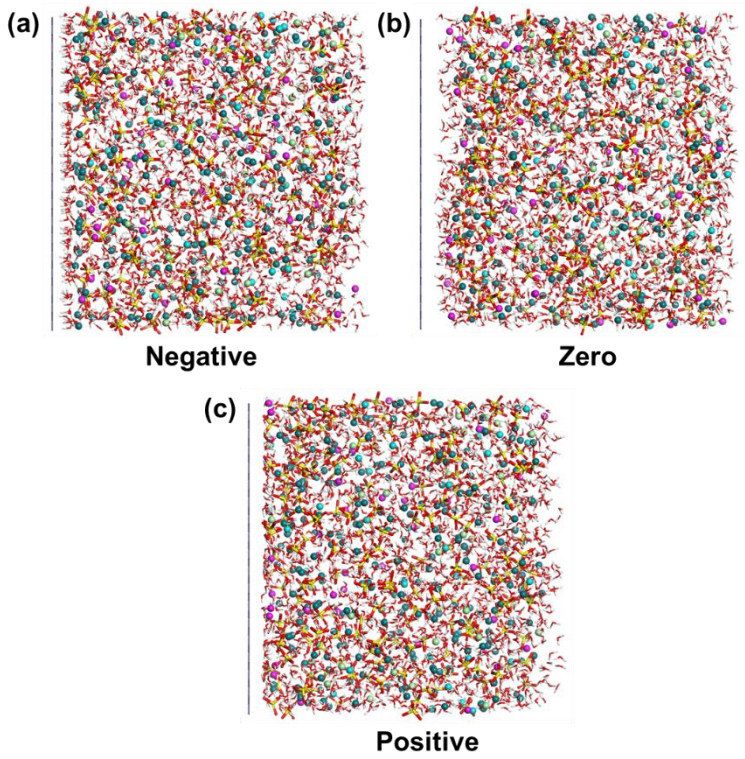


**Fig. S19** A summary of image snapshot with frontal view of the electrode-electrolyte interface in HESE system at (a) negative charge, (b) zero charge, and (c) positive charge in HESE, respectively.

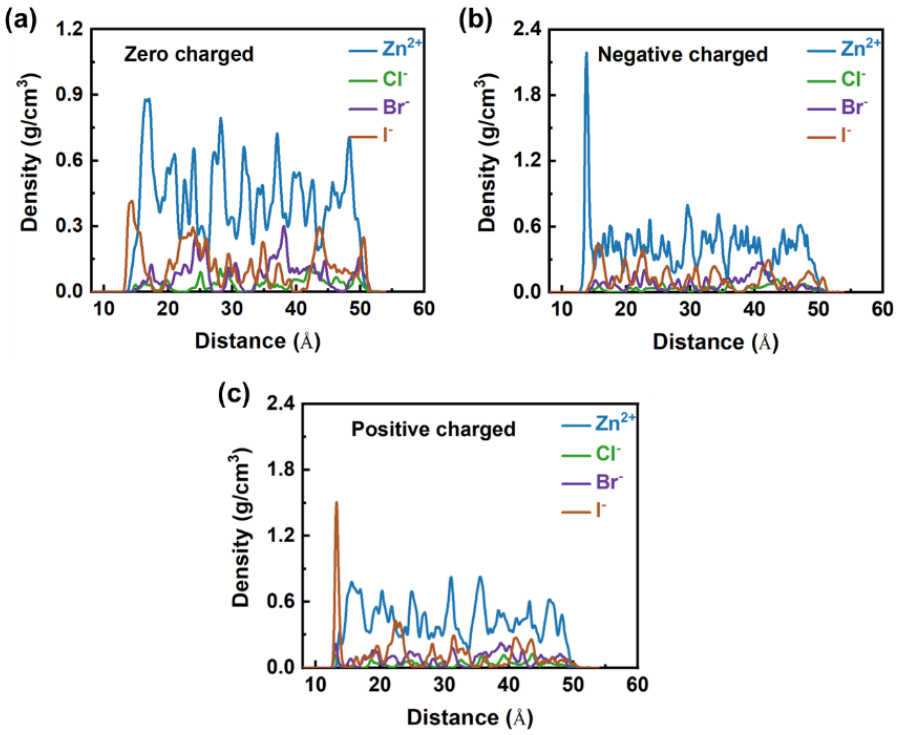


**Fig. S20** Density profiles for the $Zn^{2+}$, $Cl^-$, $Br^-$, and $I^-$ as a function of distance from Zn anode with (a) zero charge, (b) negative charge, and (c) positive charge in HESE, respectively.

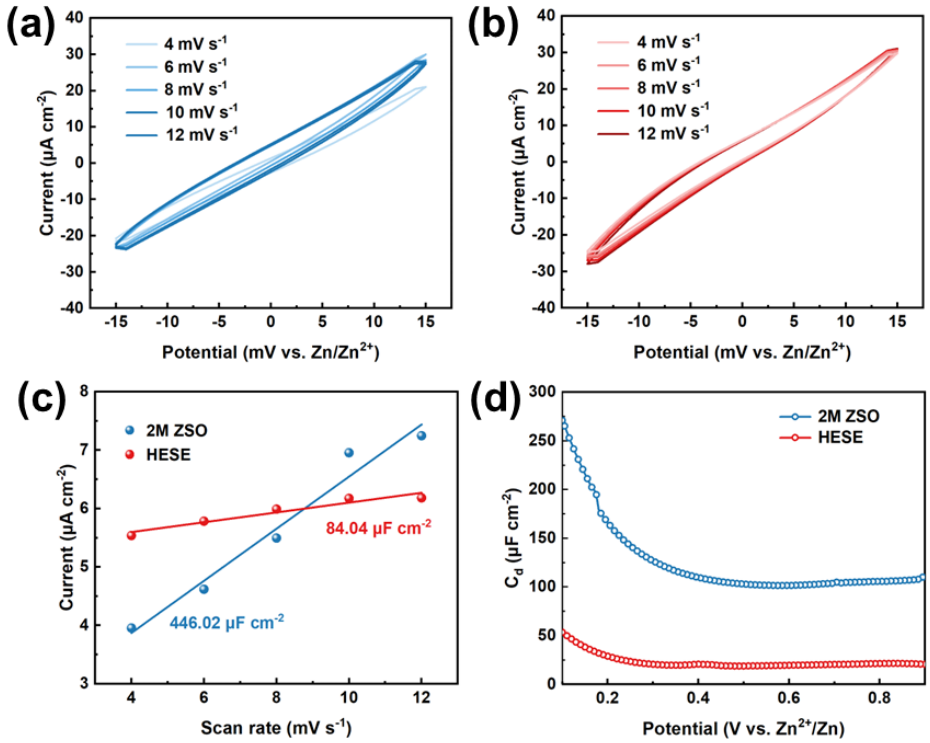


**Fig. S21** CV curves of Zn||Zn symmertic cells in (a) 2M ZSO, (b) HESE, and the linear fits to calculate (c) Electrical double-layer capacitor (EDLC), (d) Differential capacitance curves of Zn||Ti half-cells in different electrolytes

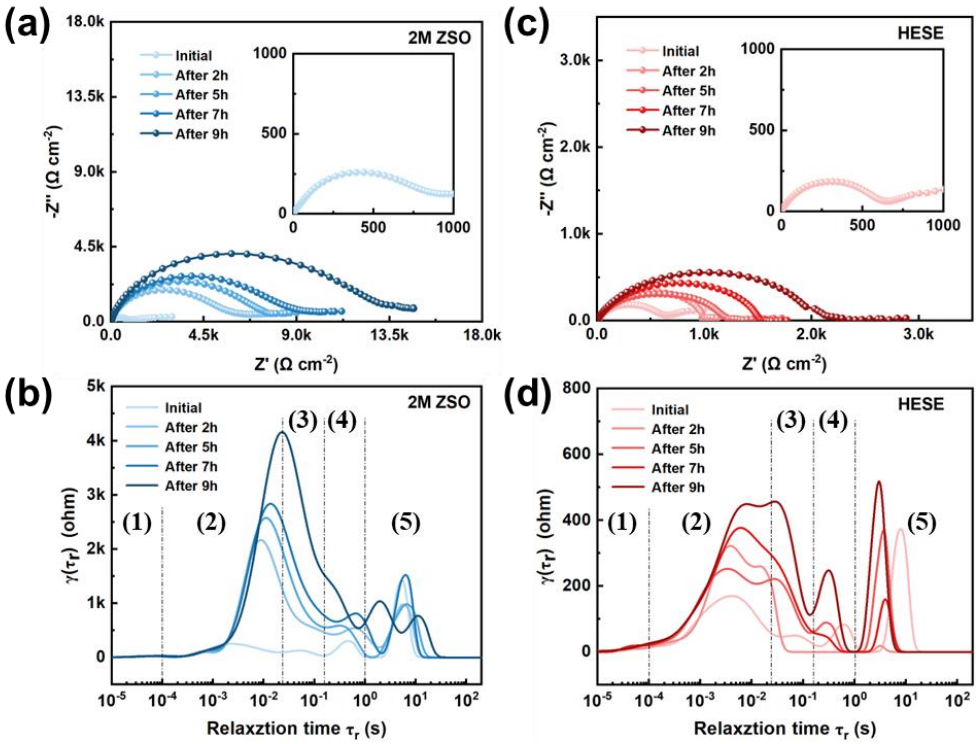


**Fig. S22** EIS and Distribution of relaxation times (DRT) fitting curves of Zn||Zn symmetric cell with (a-b) 2M ZSO, (b) HESE. (1): the relaxation of electrons, (2): the adsorption and desolvation process of $Zn(H_2O)_6^{2-}$ at the interface, (3): the migration and crystallization of Zn ions on the electrode, (4): the charge transfer process across the interface, (5): ion diffusion.

**Supplementary Note 3:** The decrease of the closed-circuit peak area of HESE is lower than that of ZSO, indicating reduced electrochemical resistance. In particular, the impedance values of adsorption and desorption processes, charge transfer processes and ion diffusion processes were reduced. Meanwhile, during the resting period of 9 h after battery assembly, the impedance of adsorption and desolution processes showed a rapid increase, indicating that the inert Zn passivation reaction kinetics was slow. In contrast, HESE helps to reduce the resistance of this process, indicating that the exposed zincophilic sites are favorable for reaction kinetics.

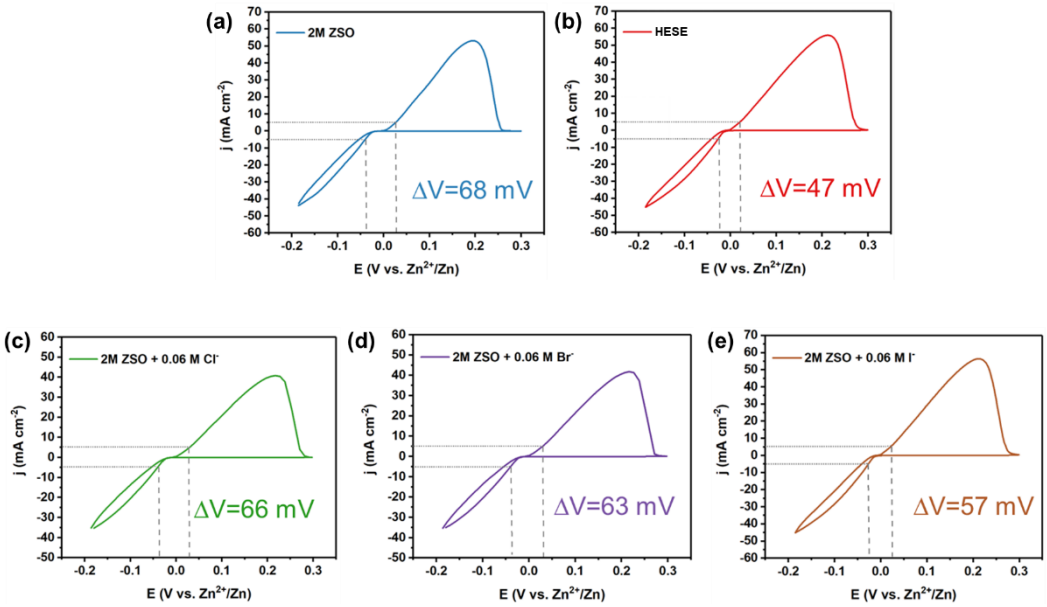


**Fig. S23** CV curves of Zn||Cu asymmetric cells in (a) 2M ZSO, (b) HESE, (c) 2M+0.06M $Cl^-$, (d) 2M+0.06M $Br^-$, and (e) 2M+0.06M $I^-$ electrolyte

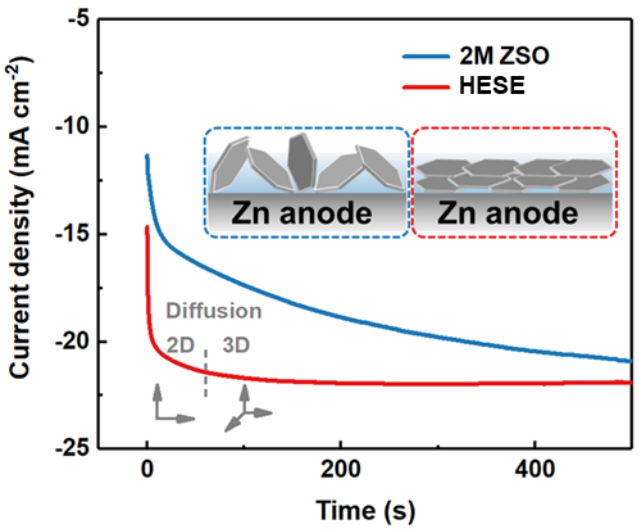


**Fig. S24** Chronoamperograms (CA) curves in different electrolytes under a overpotential of −150 mV


**Fig. S25** Digital photographs of the initial nucleation and growth processes of zinc in two electrolytes

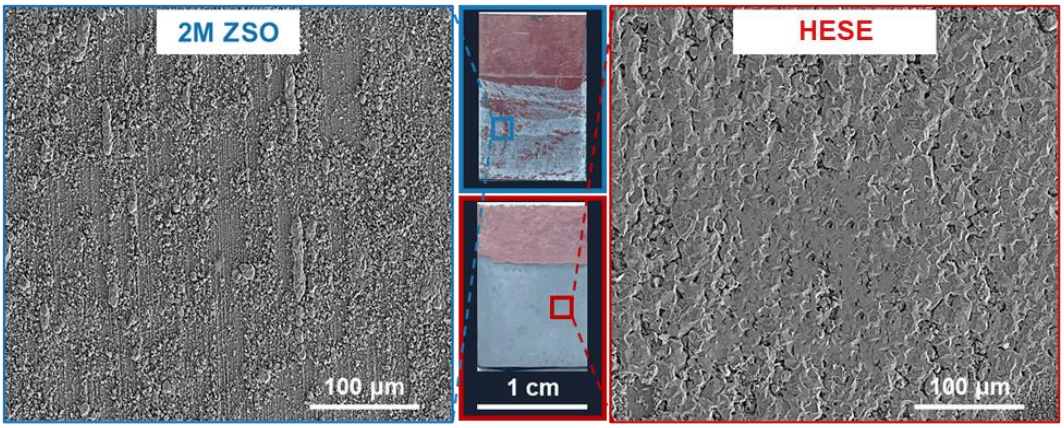


**Fig. S26** Distribution and SEM micrographs of zinc deposition (5 mAh $cm^{-2}$) on copper (Cu) substrate in two electrolytes

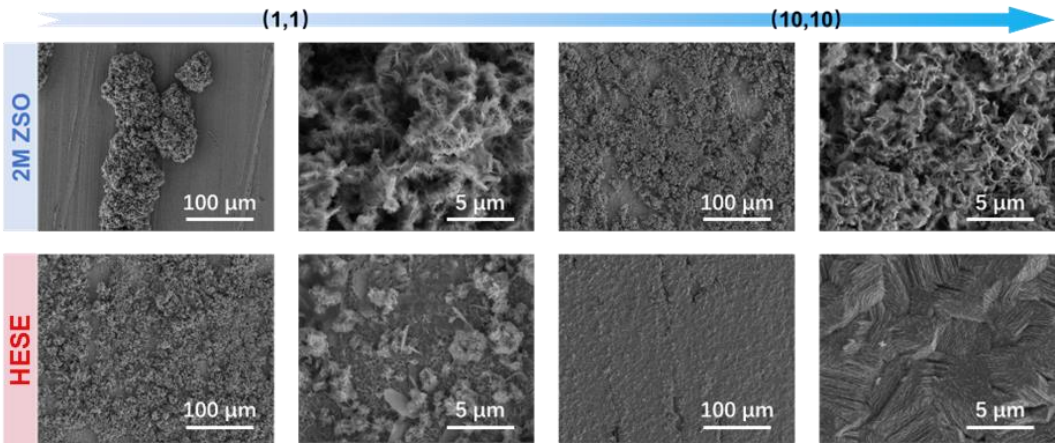


**Fig. S27** SEM images of deposited zinc morphology obtained under different deposition condition

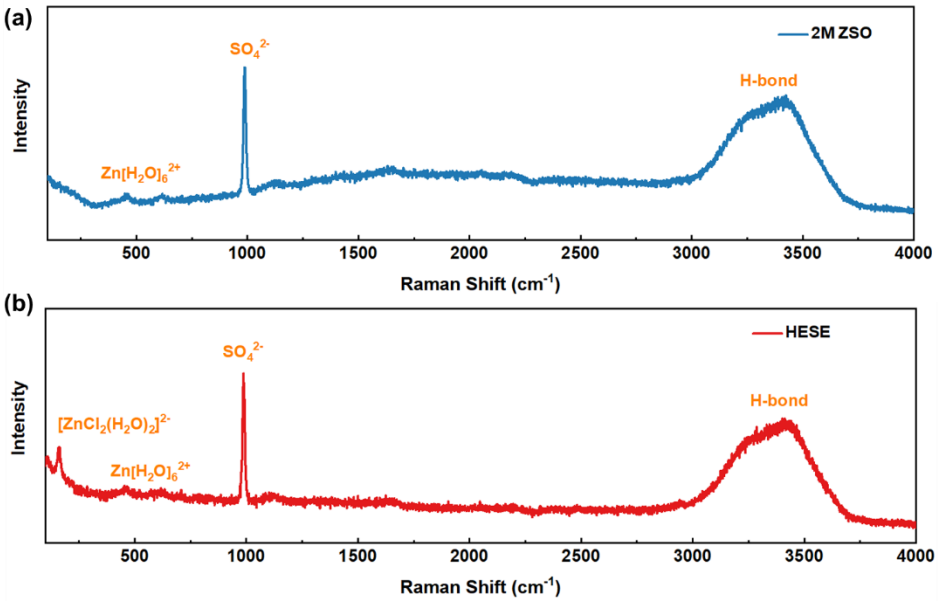


**Fig. S28** Initial Raman full-spectra of (a) 2M ZSO and (b) HESE

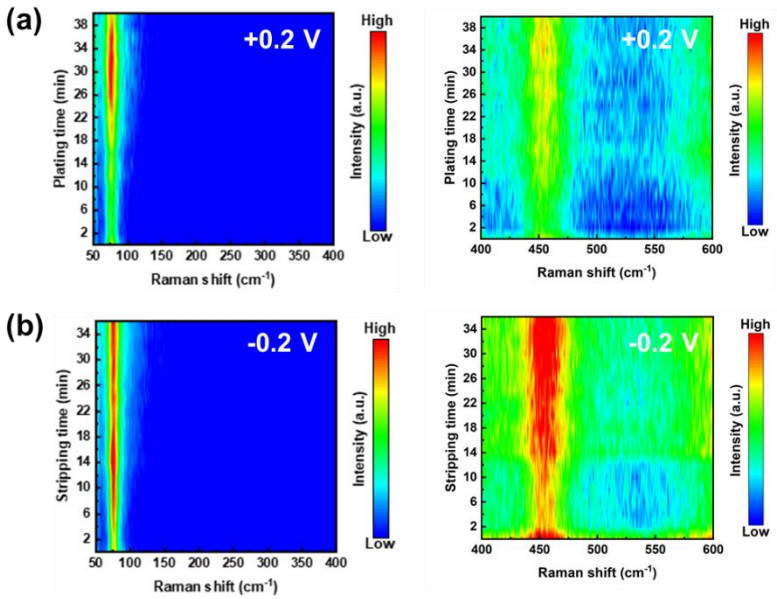


**Fig. S29** *In-situ* Raman spectra of the Zn/electrolyte interface in 2M ZSO electrolyte during (a) plating and (b) stripping

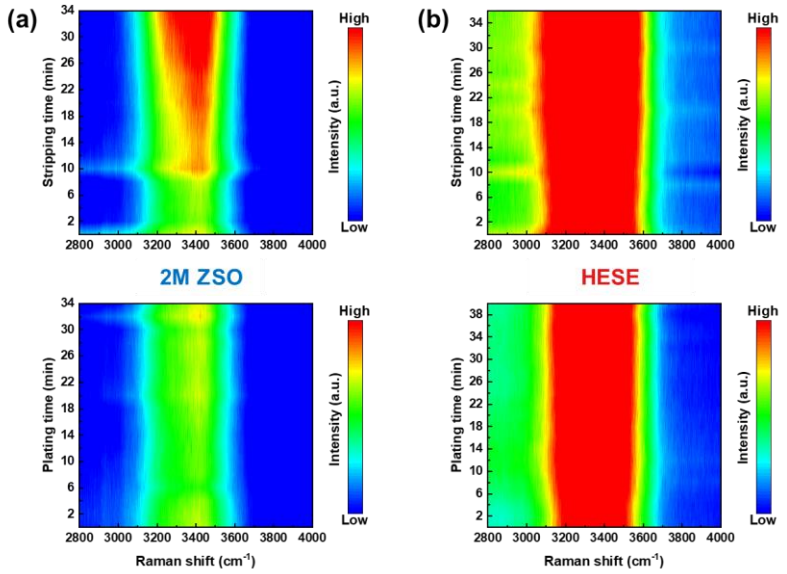


**Fig. S30** *In-situ* Raman spectra of *v*-O-H at the Zn/electrolyte interface in (a) 2M ZSO and (b) HESE during stripping and plating

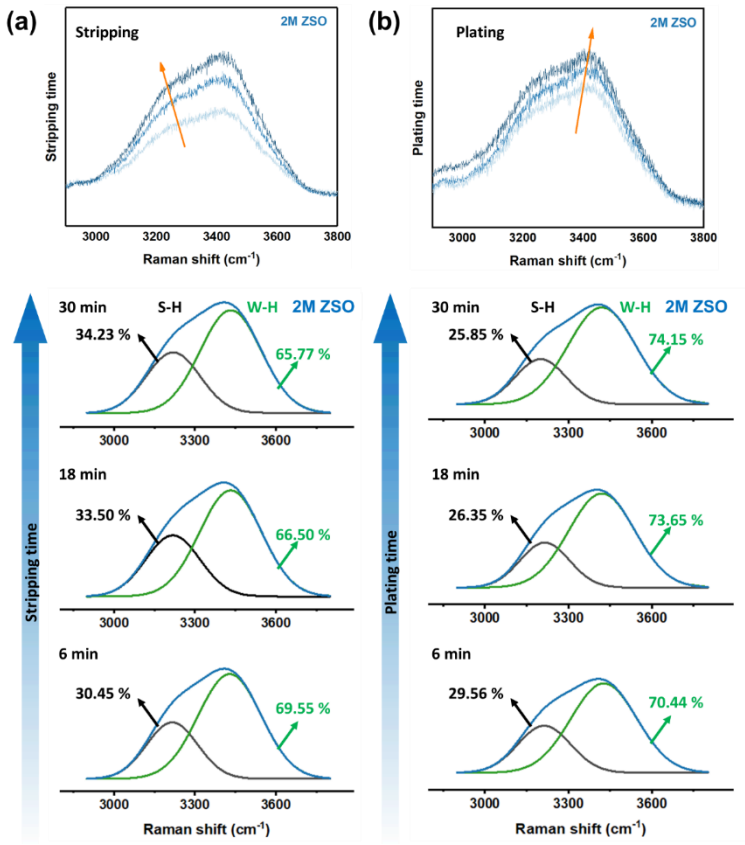


**Fig. S31** Raman spectra fitting of the *v*-O-H portion, the proportion statistics of strong and weak H-bonds (S-H and W-H) in 2M ZSO electrolyte during (a) stripping and (b) plating

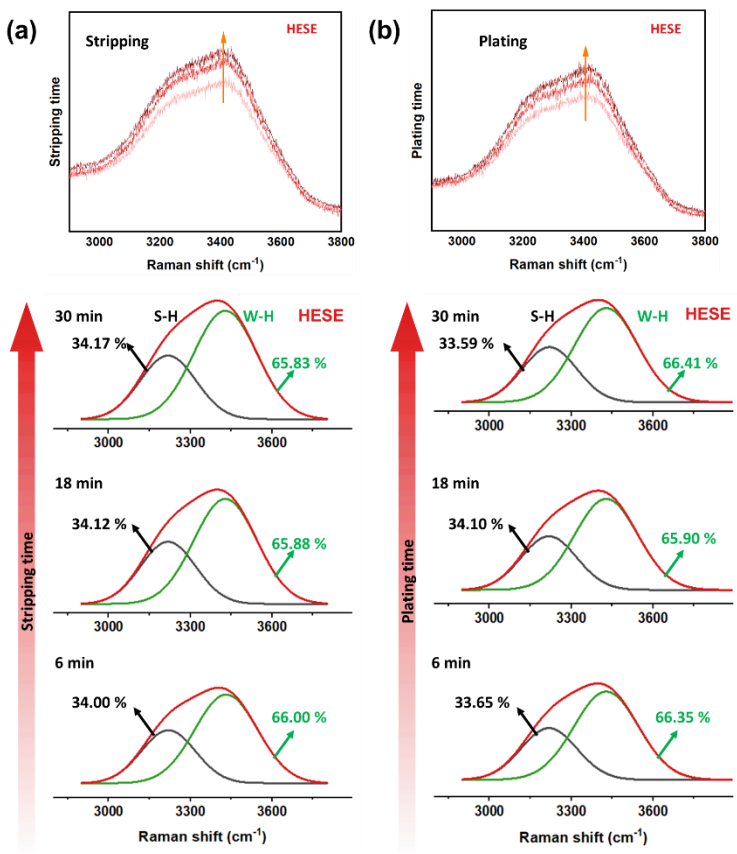


**Fig. S32** Raman spectra fitting of the *v*-O-H portion, the proportion statistics of strong and weak H-bonds (S-H and W-H) in HESE during (a) stripping and (b) plating

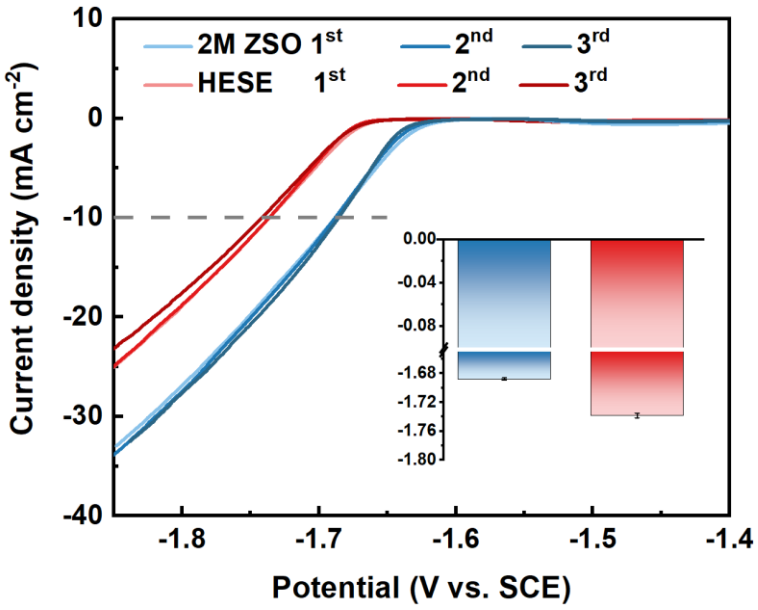


**Fig. S33** LSV curves of two electrolytes, inset is the overpotential

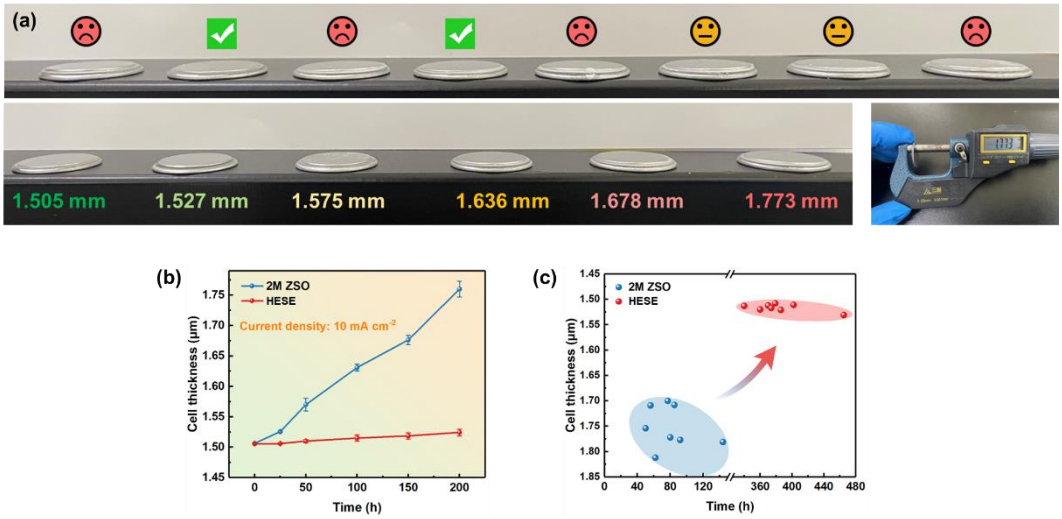


**Fig. S34** (a) Digital photos of battery expansion using 2M ZSO electrolyte and thickness changes of a single battery over time, (b) The thickness of Zn||Zn symmetric cells assembled with two electrolytes varies with the working time, (c) The regional corresponding distribution of cell thickness and cycle time

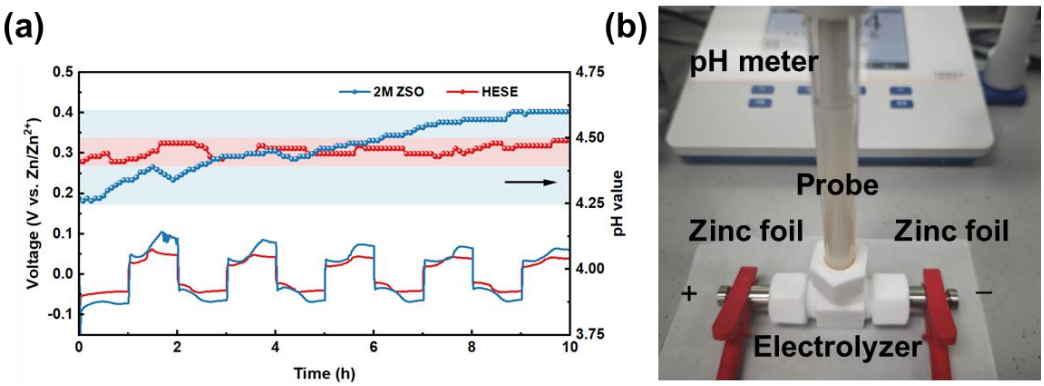


**Fig. S35** In situ pH test and device diagram during charge and discharge process

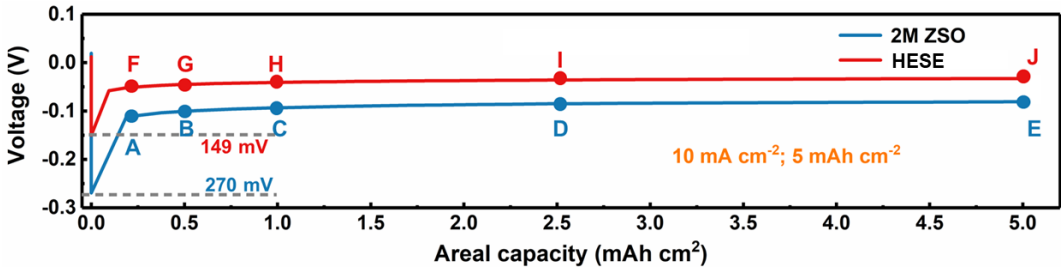


**Fig. S36** Zn deposition voltage profiles of Zn||Cu cells at 10 mA cm$^{-2}$. A-E and F-J are time nodes of different deposition capacities, which are used to observe the deposition morphology

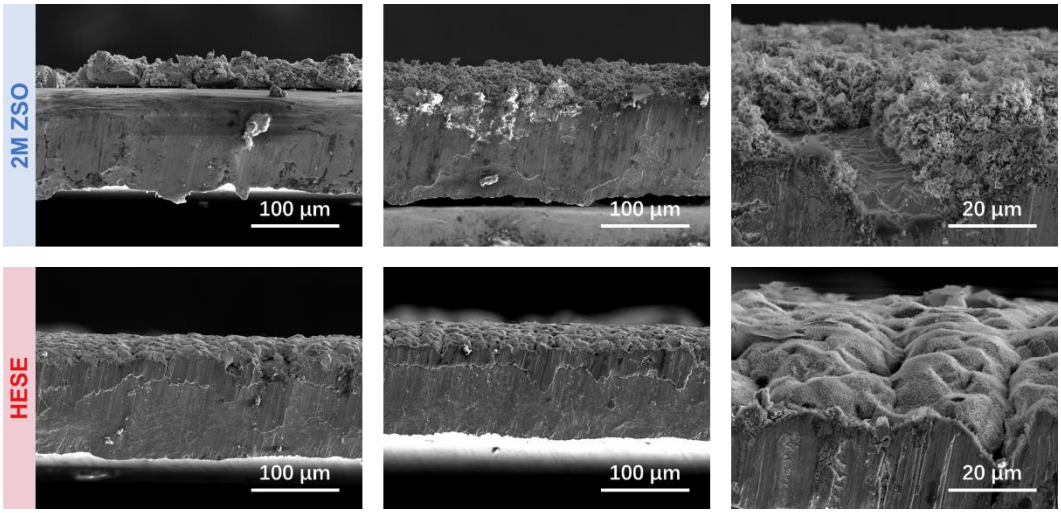


**Fig. S37** Cross-section SEM images of deposited zinc morphology

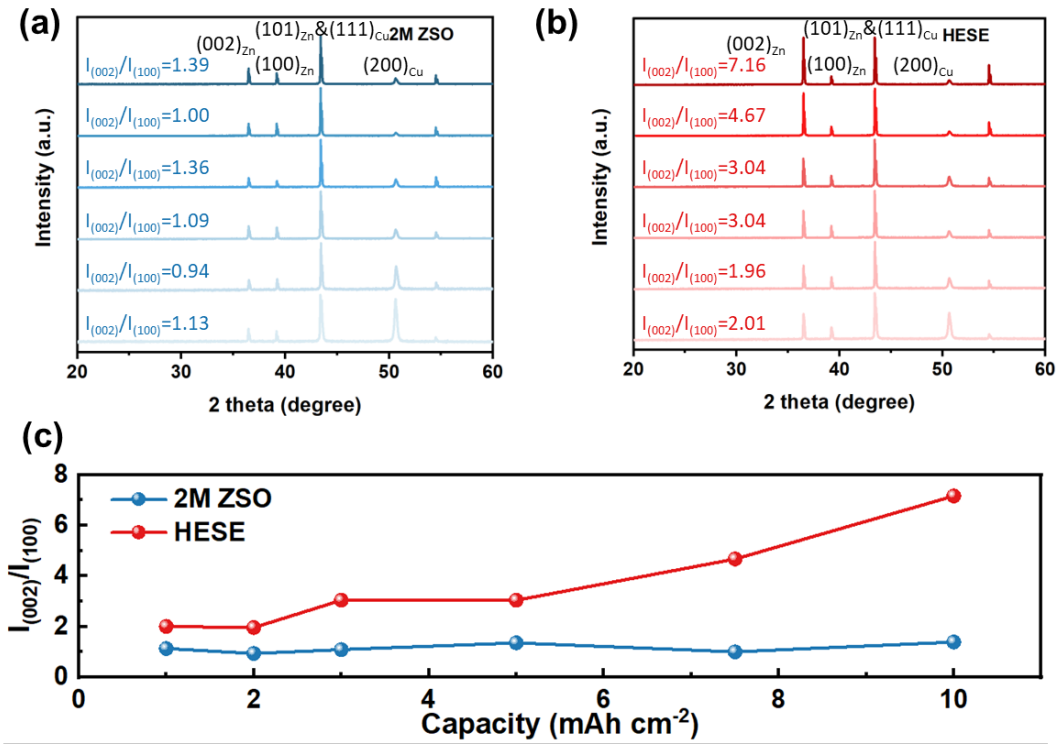


**Fig. S38** Ex-situ XRD patterns of deposited zinc with increased area capacity in (a) 2M ZSO and (b) 2HESE, (c) Proportion change of $I_{(002)}/I_{(100)}$

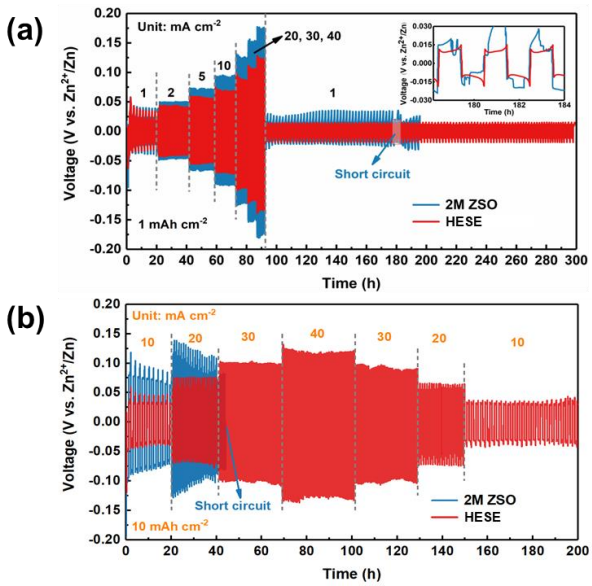


**Fig. S39** The rate performance of Zn||Zn symmetric cells with areal capacity of (a) 1 mAh $cm^{-2}$ and (b) 10 mAh $cm^{-2}$

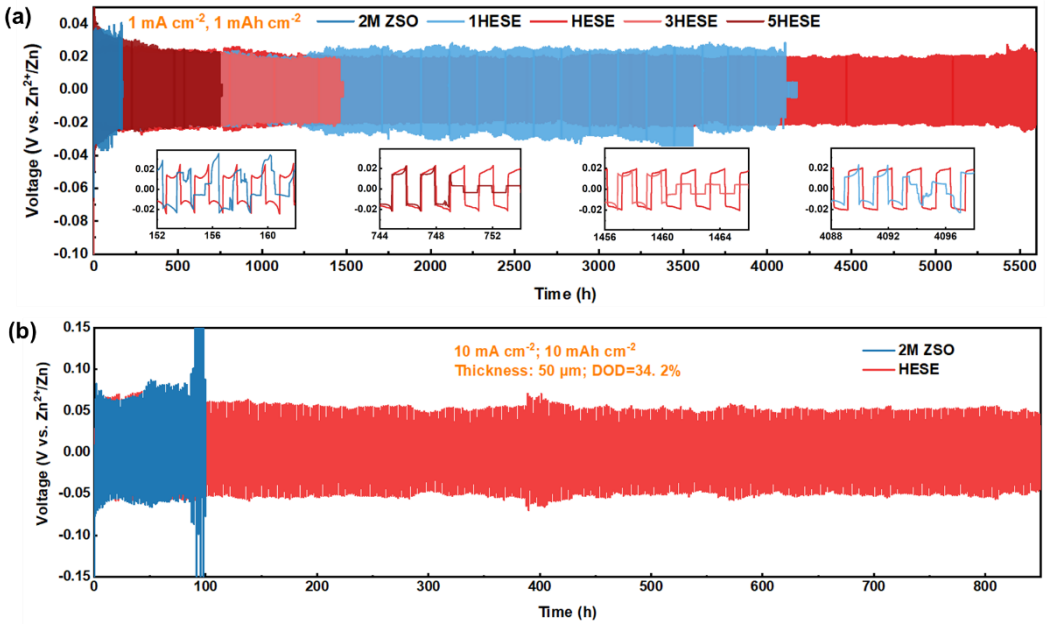


**Fig. S40** The long-cycle performance of Zn||Zn symmetric cells at (a) 1 mA cm $^{-2}$ and 1 mAh cm$^{-2}$, (b) 10 mA cm $^{-2}$ and 10 mAh cm$^{-2}$ (DOD=34.2%)

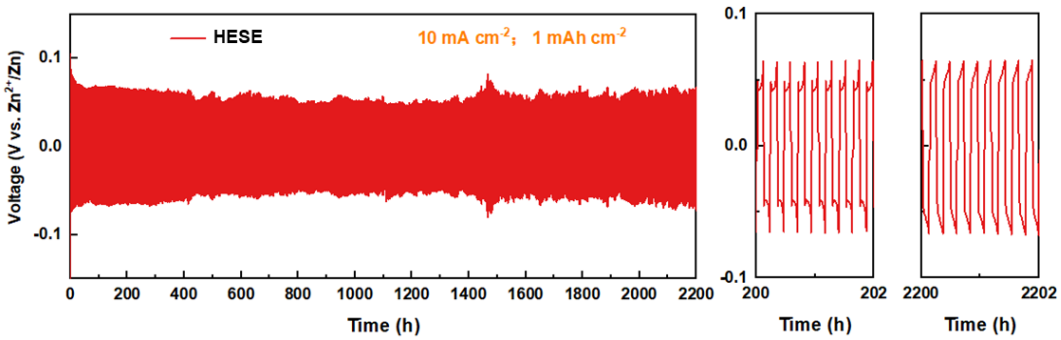


**Fig. S41** Long cycle performance and time-voltage curves of Zn||Zn symmetric cell using HESE under 10 mA $cm^{-2}$, 1 mAh $cm^{-2}$

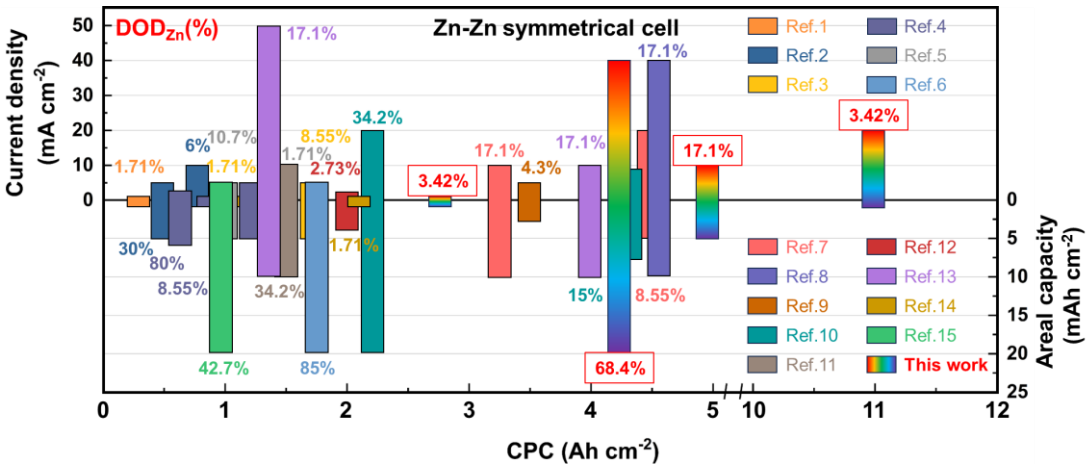


**Fig. S42** Comparison of cyclic reversibility in the recent reports.

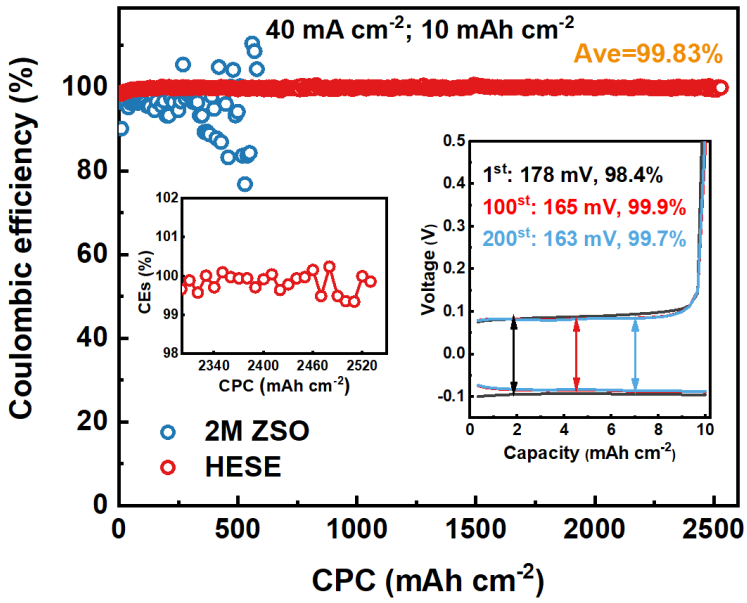


**Fig. S43** The Coulombic efficiency of Zn||Cu asymmetric cells under 40 mA $cm^{-2}$, 10 mAh $cm^{-2}$

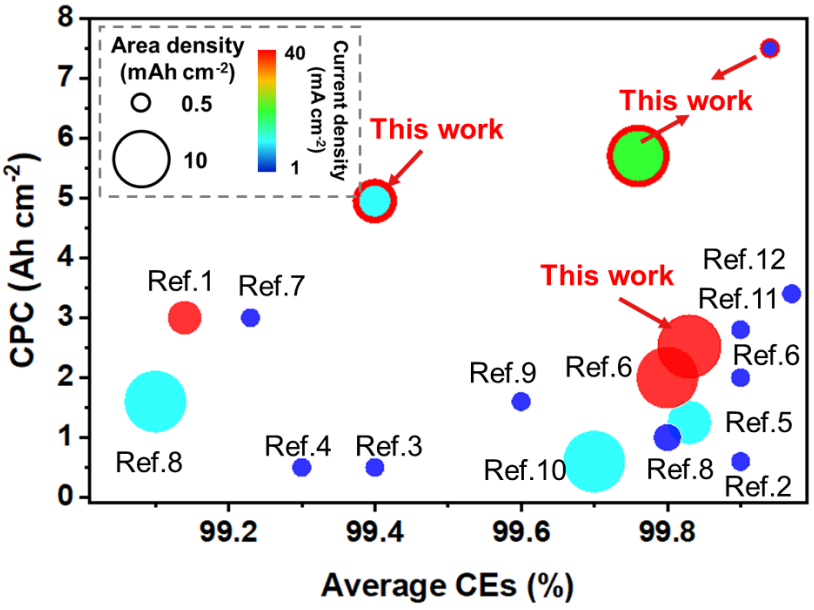


**Fig. S44** Comparison of CEs and CPC of Zn||Cu cells in the recent reports.

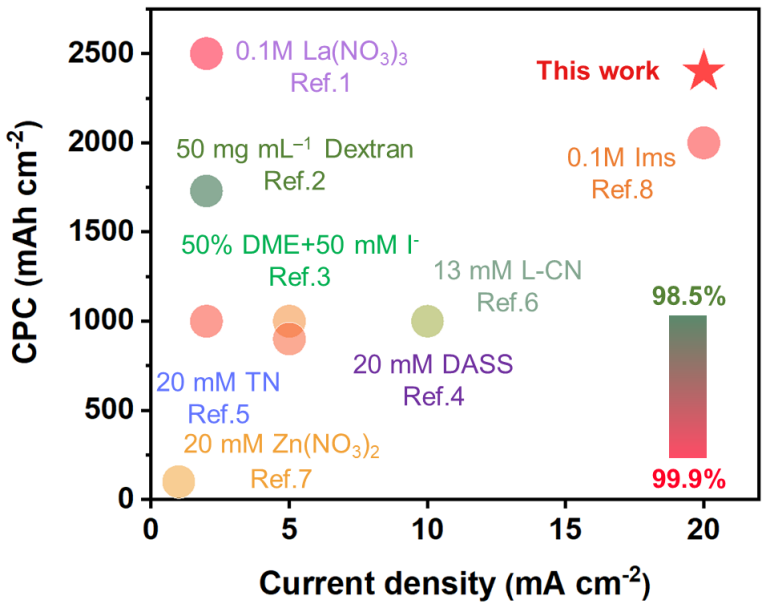


**Fig. S45** Comparison of CD and CPC of Zn||Ti cells in the recent reports.

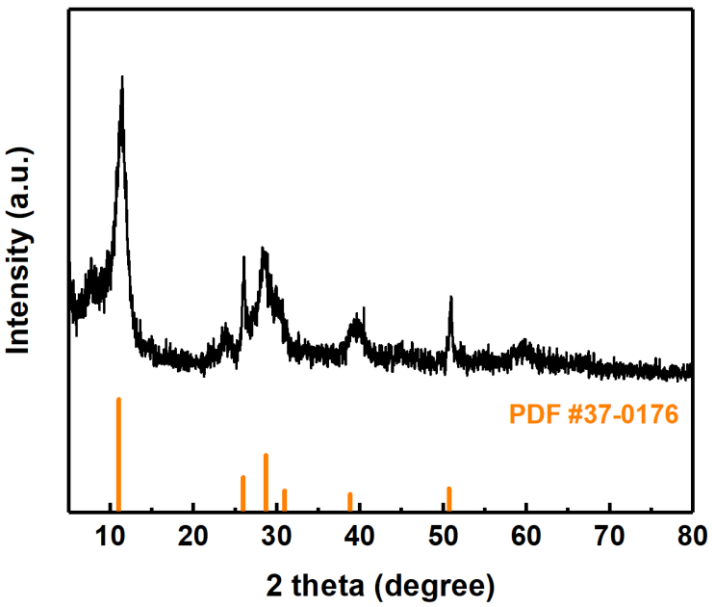


**Fig. S46** XRD pattern of $NaV_3O_8$ (NVO) powder

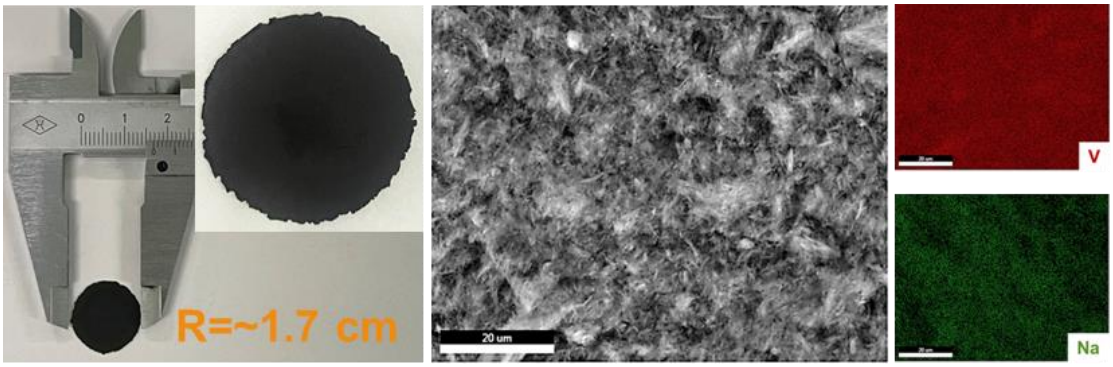


**Fig. S47** Digital photos and SEM images of high-loading (~19 mg $cm^{-2}$) cathode electrodes and mapping of key elements

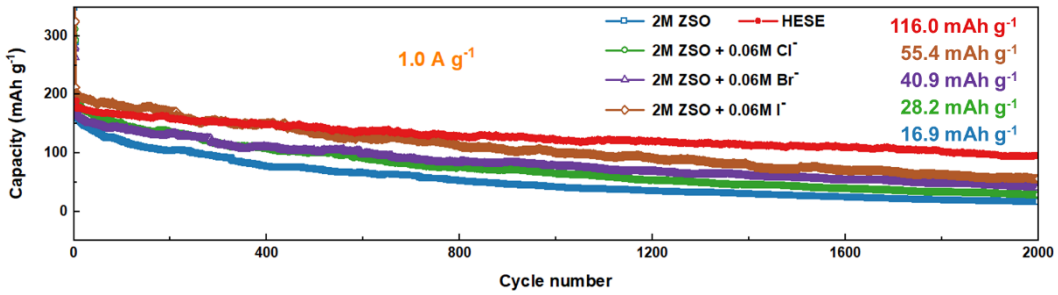


**Fig. S48** Long cycle performance of Zn||NVO full cells with different electrolytes

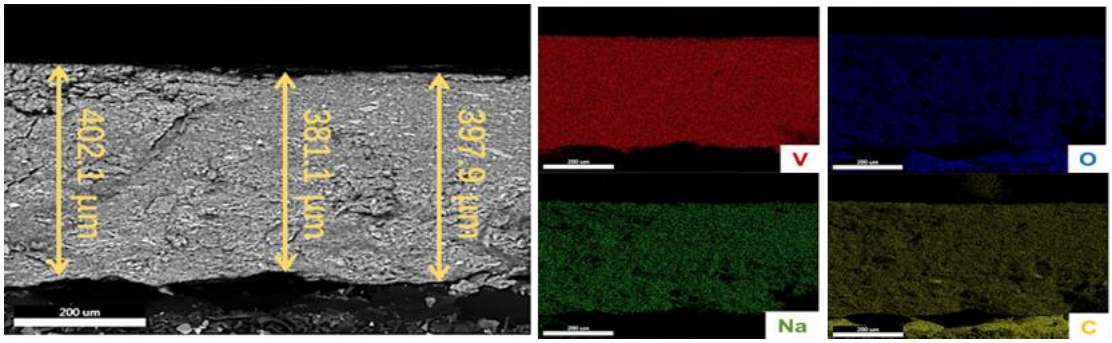


**Fig. S49** Cross-section SEM images of high-loading (~37.0 mg $cm^{-2}$) cathode electrodes and mapping of key elements

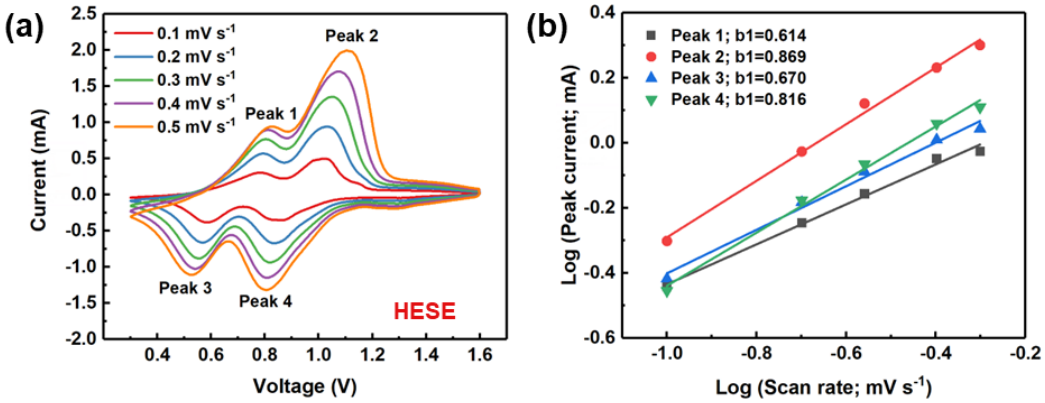


**Fig. S50** (a) CV curves at various scan rates, (b) The relations between peak current and scan rates of Zn||NVO full cell using HESE electrolyte

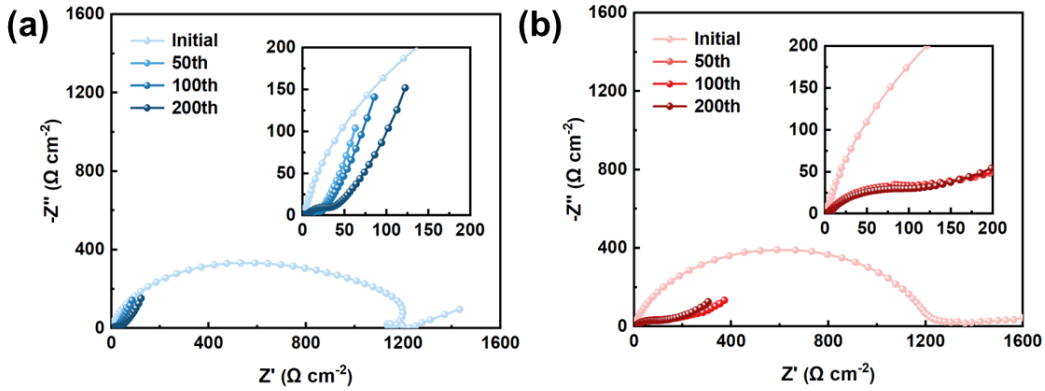


**Fig.S51** EIS curves of Zn||NVO full cell after different cycles using (a) 2M ZSO and (b) HESE

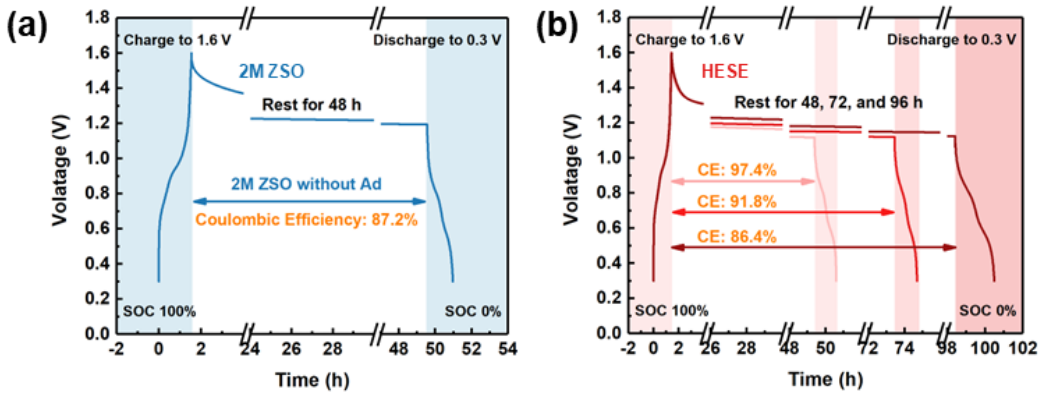


**Fig. S52** Comparison of self-discharge performances in Zn||NVO full cell with (a) 2M ZSO and (b) HESE evaluated by resting for 48, 72, 96 h at 100% state of charge (SOC), respectively

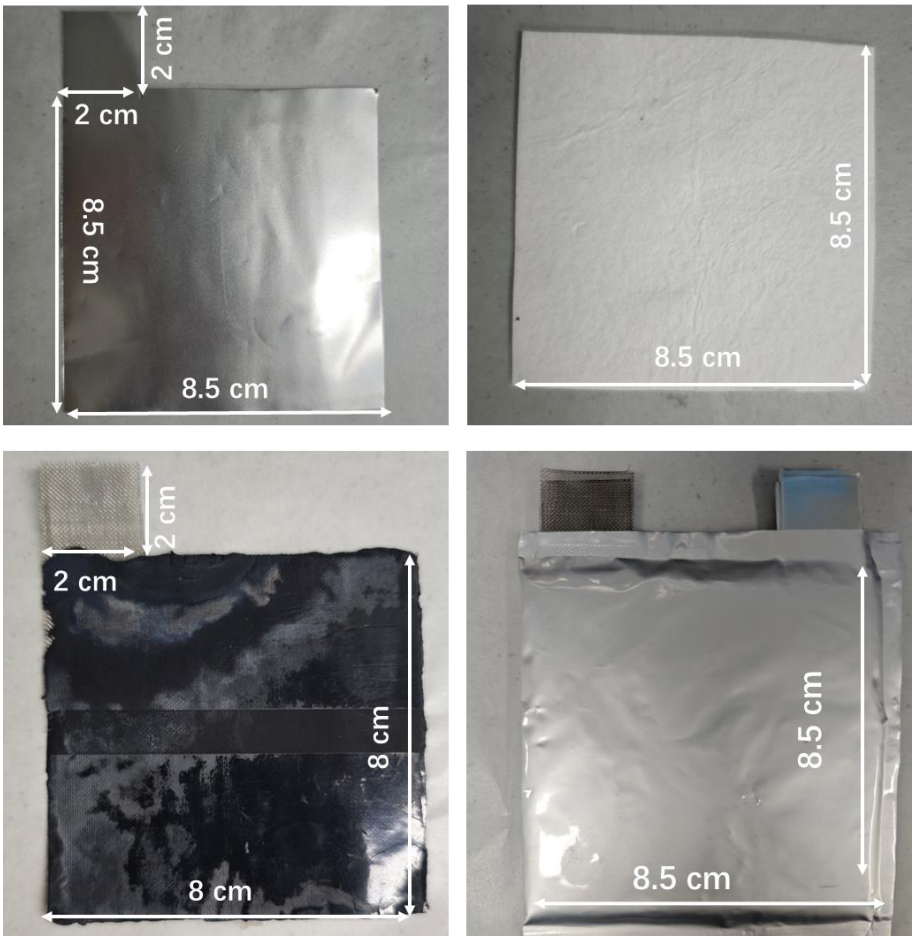


**Fig. S53** Digital photo of Ah-level multi-layer pouch cell material

**Table S1** CEs test results of different electrolytes

| Conditions | ZSO | ZSO + $Cl^-$ | ZSO + $Br^-$ | ZSO + $I^-$ | HESE |
|---|---|---|---|---|---|
| (1,5)<br>(1,1)*10 | 80.07% | 97.30% | 96.62% | 96.15% | 99.06% |
| (5,10)<br>(5,1)*60 | 92.68% | 99.17% | 99.01% | 98.83% | 99.69% |
| (5,10)<br>(5,5)*20 | / | 98.32% | 97.76% | / | 99.45% |
| Overpotential (mV) | 119.4 | 90.4 | 74.2 | 69.0 | 57.4 |

**Table. S2** The types of solvation structures and their corresponding proportion in 2M ZSO electrolyte system

| $SO_4^{2-}$-$H_2O$ | Proportion (%) |
|---|---|
| 0-6 | 30.261 |
| 1-5 | 62.364 |
| 2-4 | 2.661 |
| 3-3 | 1.973 |
| 4-2 | 1.365 |
| 5-1 | 1.015 |
| Others | 0.361 |

**Table. S3** The types of solvation structures and their corresponding proportion in HESE system

| $SO_4^{2-}$-$H_2O$-$Cl^-$-$Br^-$-$I^-$ | Proportion (%) |
|---|---|
| 0-6-0-0-0 | 3.399 |
| 1-5-0-0-0 | 1.000 |
| 1-3-1-1-0 | 10.589 |
| 1-3-1-0-1 | 11.325 |
| 1-4-0-1-0 | 20.315 |
| 1-4-1-0-0 | 24.039 |
| 1-4-0-0-1 | 10.169 |
| 2-3-0-1-0 | 1.958 |
| 2-3-1-0-0 | 1.759 |
| 2-3-0-0-1 | 1.252 |
| 2-4-0-0-0 | 0.136 |
| 0-5-1-0-0 | 4.516 |
| 0-5-0-0-1 | 3.516 |
| 0-5-0-1-0 | 4.464 |
| 1-3-0-2-0 | 0.252 |
| 1-3-2-0-0 | 0.377 |
| 1-3-0-0-2 | 0.155 |
| Others | 0.779 |

**Table. S3-2** Classified statistics

| Name | $SO_4^{2-}$-$H_2O$-($Cl^-$-$Br^-$-$I^-$) | Proportion (%) | Summary (%) |
|---|---|---|---|
| **$Zn^{2+}$-Solvent** | 0-6-(0) | 3.399 | 4.535 |
| | 1-5-(0) | 1.000 | |
| | 2-4-(0) | 0.136 | |
| **Mono-hologated CIP** | 0-5-(1) | 12.496 | 71.988 |
| | 1-4-(1) | 54.523 | |
| | 2-3-(1) | 4.969 | |
| **Multi-hologated CIP** | 1-3-(2) | 22.698 | 22.698 |
| / | Others | 0.779 | 0.779 |

**Table S4** Electrostatic potential and forming energy of main Zn solvation structure

| Name ($SO_4$-$H_2O$-Cl-Br-I) | Electrostatic potential | Formation energy (eV) |
|---|---|---|
| (0-6-0-0-0) | 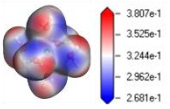 | -16.692 |
| (1-2-1-1-1) | 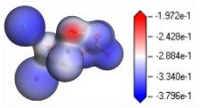 | -49.809 |
| (1-3-1-0-1) | 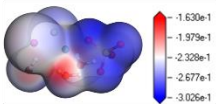 | -45.559 |
| (1-3-1-1-0) | 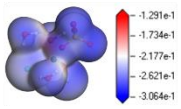 | -46.766 |
| (1-4-0-0-1) | 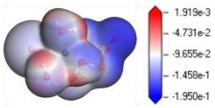 | -38.135 |

| Name ($SO_4$-$H_2O$-Cl-Br-I) | Electrostatic potential | Formation energy (eV) |
|---|---|---|
| (1-4-0-1-0) | 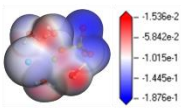 | -38.895 |
| (1-4-1-0-0) | 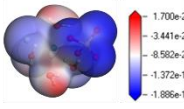 | -38.801 |
| (2-3-0-0-1) | 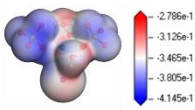 | -50.769 |
| (2-3-0-1-0) | 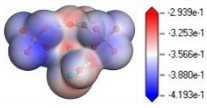 | -51.610 |
| (2-3-1-0-0) | 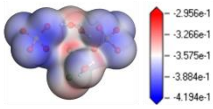 | -51.942 |

**Table S5.** Performance comparison of symmetric Zn||Zn cells from the previously reported works involving electrolyte additives and our work

| Electrolytes | Ads | mA cm$^{-2}$ mAh cm$^{-2}$ | DOD | Lifespan (h) | CPC (mAh cm$^{-2}$) | Refs. |
|---|---|---|---|---|---|---|
| 2 M $ZnSO_4$ | 8 mM $ZnF_2$ | 1/1 | 1.71% | 600 | 300 | [1] AFM 2101886[1] |
| 3 M $ZnSO_4$ | 10 mM $\alpha$-CD | 5/5 | 30.0% | 200 | 500 | [2] JACS 2022, 144, 25, 11129[2] |
| | | 10/1 | 6.0% | 160 | 800 | |
| 2 M $ZnSO_4$ | 50 mM TXA | 1/1 | 1.71% | 2100 | 1050 | [3] ESM 2023,102800[3] |
| | | 5/5 | 8.55% | 700 | 1750 | |
| 2 M $ZnSO_4$ | 1% Py | 1/1 | 1.71% | 1820 | 910 | [4] Angew e202302302[4] |
| | | 5/5 | 8.55% | 550 | 1375 | |
| | | 2/6.3 | 80% | 575 | 575 | |
| 1 M $ZnSO_4$ | 0.2 M KI | 1/1 | 2.1% | 3000 | 1500 | [5] Small 2023, 2207664[5] |
| | | 5/5 | 10.7% | 400 | 1000 | |
| 2 M $ZnSO_4$ | 0.1 M Ims | 1/1 | 1.71% | 3500 | 1750 | [6] EES 2022, 15, 4748[6] |
| | | 5/5 | 8.54% | 400 | 1000 | |
| | | 10/20 | 85% | 350 | 1750 | |
| 2 M $ZnSO_4$ | 20 mM $CH_3COONH_4$ | 10/10 | 17.1% | 650 | 3250 | [7] AS 2201433[7] |
| | | 20/5 | 8.55% | 450 | 4500 | |
| | | 20/20 | 34.2% | 130 | 1300 | |
| 2 M $ZnSO_4$ | 2g $L^{-1}$ $CeCl_3$ | 40/10 | 17.1% | 180 | 3600 | [8] AM 2203104[8] |
| 2 m Zn(OTf)2 | 7 M DEC | 5/2.5 | 4.3% | 3500 | 3500 | [9] ACS Nano 2022, 16 (6), 9667[9] |
| 2 M $ZnSO_4$ | 1.5 wt% L-CN | 8.85/8.85 | 15% | 975 | 4310 | [10] EES 2023,16, 2684[10] |
| | | 20/20 | 34.2% | 220 | 2200 | |
| 1 M $ZnSO_4$ | 2 wt.% PDD | 1/1 | 3.42% | 3000 | 1500 | [11] Angew 202302701[11] |
| | | 10/10 | 34.2% | 300 | 1500 | |
| 2 M $Zn(OTf)_2$ | Hybrid eutectic co-solvents | 2/4 | 2.73% | 2000 | 2000 | [12] NC 2023 14, 3067 Swagelok-type cells[12] |
| | | 2/8 | 5.47% | 1600 | 1600 | |
| 1 m $Zn(CF_3SO_3)_2$ | 50 mg $mL^{-1}$ Dextran | 10/10 | 17.1% | 800 | 4000 | [13] AEM 2301743[13] |
| | | 50/10 | 17.1% | 55 | 1375 | |
| 2 M $ZnSO_4$ | 0.1 M L-Asp | 1/1 | 3.42% | 4260 | 2130 | [14] AEM 2301670[14] |
| | | 10/10 | 85.5% | 240 | 1200 | |
| 2 M $Zn(TFMS)_2$ | 50% $H_2O$+50% DME+50 mM $I^-$ | 1.77/1.77 | 10% | 5000 | 4425 | [15] Angew e202309594[15] |
| | | 5/20 | 42.7% | 400 | 1000 | |
| | | 8.85/13.35 | 75.5% | 300 | 1335 | |
| **2 M $ZnSO_4$** | **0.02 M $Cl^-$,$Br^-$,$I^-$** | **1/1** | **3.42%** | **5600** | **2800** | **This work** |
| | | **10/5** | **17.1%** | **1000** | **5000** | |
| | | **10/10** | **34.2%** | **850** | **4250** | |
| | | **20/1** | **3.42%** | **1500** | **11000** | |
| | | **40/20** | **68.4%** | **210** | **4200** | |

Note: [*x*] corresponding to the annotation in Fig.S42.

**Table S6.** Performance comparison of Zn||Cu cells from the previously reported works involving electrolyte additives and our work

| Electrolytes | Ads | mA cm$^{-2}$<br>mAh cm$^{-2}$ | DOD<br>(%) | CPC (mAh cm$^{-2}$)<br>CE | Refs. |
|---|---|---|---|---|---|
| 2 M $ZnSO_4$ | 0.08 M $ZnF_2$ | 40/3.0 | / | 3000/99.14% | [1] AFM 2101886[1] |
| 3 M $ZnSO_4$ | 10 mM $\alpha$-CD | 1/1 | / | 600/99.90% | [2] JACS 2022 144, 25[2] |
| 2 M $ZnSO_4$ | 50 mM TXA | 5/1 | / | 500/99.4% | [3] ESM 2023 102800[3] |
| 2 M $ZnSO_4$ | 1% Py | /<br>2/1 | / | 1200/99.50%<br>500/99.3% | [4] Angew e202302302[4] |
| 1 M $ZnSO_4$ | 0.2 M KI | 10/5 | 10.7% | 1250/99.83% | [5] Small 2023, 2207664[5] |
| 2 M $ZnSO_4$ | 0.1 M Ims | 5/1<br>40/10 | 1.71%<br>17.1% | 2000/99.9%<br>2000/99.8% | [6] EES 2022, 15, 4748[6] |
| 2 M $ZnSO_4$ | 20 mM $CH_3COONH_4$ | 2/1 | / | 3000/99.23% | [7] AS 2201433[7] |
| 1 M $ZnSO_4$ | 2wt.% PDD | 2/2<br>10/10 | 6.84%<br>34.2% | 1000/99.8%<br>1600/99.1% | [8] Angew 202302701[11] |
| 2 M $ZnSO_4$ | 0.1 M L-Asp | 1/1 | 3.42% | 1600/99.6% | [9] AEM 2301670[14] |
| 2 M $ZnSO_4$ | 2g $L^{-1}$ $CeCl_3$ | 10/10 | / | 600//99.7% | [10] AM 2203104[8] |
| $ZnSO_4$ | Gel/SA-acetate | 1/1 | / | 2800/99.9% | [11] Angew 2310970[16] |
| 1 M $Zn(CF_3SO_3)_2$ | 50 mg $mL^{-1}$ Dextran | 5/1 | 1.71 | 3400/99.97% | [12] AEM 2301743[13] |
| **2 M $ZnSO_4$** | **0.02 M $Cl^-$,$Br^-$,$I^-$** | **5/1**<br>**20/10**<br>**40/10** | **3.42%**<br>**34.2%**<br>**34.2%** | **7800/99.94%**<br>**5700/99.76%**<br>**2520/99.83%** | **This work** |

Note: [*x*] corresponding to the annotation in Fig. S44.

**Table S7.** Performance comparison of Zn||Ti cells from the previously reported works involving electrolyte additives and our work

| Electrolytes | Ads | mA cm$^{-2}$ mAh cm$^{-2}$ | DOD (%) | CPC (mAh cm$^{-2}$) CE | Refs. |
|---|---|---|---|---|---|
| 2 M $ZnSO_4$ | 0.1 M Ims | 20/10 | 17.1% | 2000/99.70% | EES, 2022, 15, 4748[6] |
| 3 M $Zn(CF_3SO_3)_2$ | 20 mM $Zn(NO_3)_2$ | 1/0.5 | / | 100/99.40% | Angew 2021, 60, 13035[17] |
| 1 M $Zn(CF_3SO_3)_2$ | 50 mg mL$^{-1}$ Dextran | 2/1 | 3.42% | 1730/98.54% | AEM 2301743[13] |
| 2 M $Zn(TFMS)_2$ | 50% $H_2O$+50% DME+50 mM $I^-$ | 2/1 | 5.7% | 1000/99.66% | Angew e202309594[15] |
| 2 M $ZnSO_4$ | 0.1M $La(NO_3)_3$ | 2/1 | / | 2500/99.9% | NC 2022, 13, 3252[18] |
| 2 M $ZnSO_4$ | 13 mM L-CN | 10/1 | / | 1000/98.85% | EES 2023,16, 2684[10] |
| 2 M $ZnSO_4$ | 0.02 M DASS | 5/5 | / | 1000/99.44% | AEM 202302770[19] |
| 2 M $ZnSO_4$ | 20 mM TN | 5/1 | / | 900//99.60% | AFM 202311773[20] |
| **2 M $ZnSO_4$** | **0.02 M $Cl^-$,$Br^-$,$I^-$** | **20/10** | **34.2%** | **2400/99.64%** | **This work** |

**Table S8.** Performance comparison of full cells from the previously reported works involving electrolyte additives and our work

| Electrolytes | Ads | Cathode | Cycles Retention | Capacity/mAh $g^{-1}$ | N:P | Refs. |
|---|---|---|---|---|---|---|
| 2 M $ZnSO_4$ | 0.08 M $ZnF_2$ | $LiMn_2O_4$ | 100/75.64% | 0.2 A $g^{-1}$/77.3 | >100 | AFM 2101886[1] |
| 3 M $ZnSO_4$ | 10 mM $\alpha$-CD | $V_2O_5$ | 800/84.2% | 3.0 A $g^{-1}$/325 | 11 | JACS 2022, 144, 11129[2] |
| 2 M $ZnSO_4$ | 50 mM TXA | $NH_4V_4O_{10}$ | 500/85.9% | 1 A $g^{-1}$/146.1 | >100 | ESM 2023, 59, 102800[3] |
| 2 M $ZnSO_4$ | 1% Py | $NaV_3O_8$ | 550/91.3% | 4.0 A $g^{-1}$/125 | 2.1 | Angew e202302302[4] |
| 1 M $ZnSO_4$ | 0.2 M KI | AC | 2000/81.64 | 4.0 A $g^{-1}$/169 | / | Small 2023, 2207664[5] |
| 2 M $ZnSO_4$ | 0.1 M Ims | $NaV_3O_8$ | 540/91.15%<br>1000/96%<br>3000/88% | 0.5 A $g^{-1}$/302.5<br>4.0 A $g^{-1}$/95.3<br>20.0 A $g^{-1}$/159 | 12.15<br>4.81<br>>10 | EES 2022, 15, 4748[6] |
| 3 M $Zn(CF_3SO_3)_2$ | 20 mM $Zn(NO_3)_2$ | $MnO_2$ | 700/96.5% | 10 C/133.4 | / | Angew 2021, 60, 13035[17] |
| 2 M $ZnSO_4$ | 0.1 M L-Asp | PEDOT-$V_2O_5$ | 1000/91.6% | 10A $g^{-1}$/320 | 40 | AEM 2301670[14] |
| **2 M $ZnSO_4$** | **0.02 M $Cl^-$,$Br^-$,$I^-$** | **$NaV_3O_8$** | **1000/91.3%**<br>**3000/85.4%** | **4.0 A $g^{-1}$/153.4**<br>**10.0 A $g^{-1}$/151** | **1.52**<br>**6.54** | **This work** |

| Electrolytes | Method | Cathode | Cycles Retention | Capacity/mAh $cm^{-2}$ | N:P | E/C | Wh $kg^{-1}$ | Refs. |
|---|---|---|---|---|---|---|---|---|
| 2 M $ZnSO_4$ | FCOF@Zn | $MnO_2$ | 250/0.5mAh $cm^{-2}$ | 3 mA $cm^{-2}$/2.0 | ~2 | 12 μL $mAh^{-1}$<br>3.7 μL $mg^{-1}$ | 55/130 | NC 2021 12:6606[21] |
| 2 M $Zn(OTf)_2$ | Hybrid eutectic co-solvents | ZnVO<br>AC | 250/~90%<br>300/~88% | 45 mA $g^{-1}$/4.4<br>45 mA $g^{-1}$/3.2 | 1.08<br>2.15 | 4.7 μL $mg^{-1}$<br>8.1 μL $mg^{-1}$ | 7.3/45.1<br>9.7/82.5 | NC 2023 14:3067[12] |
| 2 M $ZnSO_4$ | 1% Py | $NaV_3O_8$ | / | / | 4.5<br>2.1 | 9.2 μL $mg^{-1}$<br>20 μL $mg^{-1}$ | x/64<br>x/37.5 | Angew e202302302[4] |
| 2 M $ZnSO_4$ | 0.1 M L-Asp | PEDOT-$V_2O_5$ | 200/84.4% | 0.05A $g^{-1}$/4.62 | 2.4 | 12 μL $mAh^{-1}$<br>4.5 μL $mg^{-1}$ | 41.1/119.8 | AEM 2301670[14] |
| 2 M $ZnSO_4$ + 0.1 M $MnSO_4$ | Stress-governed VVLP separator | $MnO_2$ | 200/61.8%<br>80/71.9%(pouch) | 3.2 mA $cm^{-2}$/14.78<br>1.6 mA $cm^{-2}$/17.43 | 3.74<br>1.35 | 2.5 μL $mAh^{-1}$<br>0.77 μL $mg^{-1}$ | x/47.6<br>x/115.1 | EES 2023,16, 2133[22] |
| **2 M $ZnSO_4$** | **0.02 M $Cl^-$,$Br^-$,$I^-$** | **$NaV_3O_8$** | **100/~94.7%** | **1.0 A $g^{-1}$/9.23** | **~2** | **6 μL $mAh^{-1}$**<br>**2.4 μL $mg^{-1}$** | **57.6/152.2** | **This work** |
| **2 M $ZnSO_4$** | **0.02 M $Cl^-$,$Br^-$,$I^-$** | **$NaV_3O_8$** | **1500/~80.4%** | **4.0A $g^{-1}$/2.92** | **1.52** | **12 μL $mAh^{-1}$**<br>**5.3 μL $mg^{-1}$** | **19.5/84.5** | |

**Table S9.** Battery design parameters for zinc ion full cell based onZn||NVO in HESE

| Name | Material | NaVOH |
|---|---|---|
| Cathode | Discharge capacity / mAh $g^{-1}$ | 232 (1A $g^{-1}$, after 100 cycle) |
| | Active material loading / % | 70 |
| | Cathode weight / mg $cm^{-2}$ | 37.00 |
| | Areal capacity / mAh $cm^{-2}$ | 9.23 |
| Separator | Radius/ cm; Weight / mg | 1.9; 15.60 |
| Electrolyte | Volume / μL; Weight / mg | 90; 119.43 |
| Zn Anode | Radius/ cm; Weight / mg | 1.2; 40.40 |
| N:P | / | ~2 |
| Working voltage | V | ~1.2 |

$M=m_C+m_S+m_E+m_A$

$=37.00/0.7+15.6/(3.14\times0.95^2)+119.43+40.40/(3.14\times0.6^2)$

$=52.86+5.50+119.43+35.74$

$=213.53$ mg $cm^{-2}$

$W_{electrode}=U\times9.23/m_{electrode}$

$=1.2\times9.23/(37+35.74)$

$=152.2$ Wh $kg^{-1}$

**Table S10.** COSTING. Summary of prices of various reagents of one coin cell. Price data of all this were collected from Internet (https://www.alibaba.com/)

| Name | Online Price | Molecular weight | Consumption of per $cm^2$ | Total cost ($) |
|---|---|---|---|---|
| $ZnSO_4 \cdot 7H_2O$ | 0.6 \$ $kg^{-1}$ | 287.5 | 51.76 mg | $31.056\times10^{-6}$ |
| $ZnCl_2$ | 1.12 \$ $kg^{-1}$ | 136.3 | 0.74 mg | $0.829\times10^{-6}$ |
| $ZnBr_2$ | 2.0 \$ $kg^{-1}$ | 225.2 | 1.22 mg | $2.440\times10^{-6}$ |
| $ZnI_2$ | 2.0 \$ $kg^{-1}$ | 319.2 | 1.72 mg | $1.720\times10^{-6}$ |
| DZ | 0.1 \$ $kg^{-1}$ | 18 | 63.99 mg | $6.399\times10^{-6}$ |
| Cathode (NVO) ($V_2O_5$+NaCl) | (M=1:3.51) 150+0.05 \$ $kg^{-1}$ | / | 37.00 mg | $12.320\times10^{-4}$ |
| Cathode (C) | 25 \$ $kg^{-1}$ | / | 10.57 mg | $26.425\times10^{-5}$ |
| Cathode (PTFE) | 7.2 \$ $kg^{-1}$ | / | 5.29 mg | $38.088\times10^{-6}$ |
| Separator (GF/A) | 50.5 \$ $kg^{-1}$ | / | 5.50 mg | $27.775\times10^{-5}$ |
| Anode (Zn,50μm) | 2.5 \$ $kg^{-1}$ | / | 35.74 mg | $89.350\times10^{-5}$ |
| Current collector (SS) | 0.8 \$ $m^{-2}$ | / | 91.50 mg | $73.200\times10^{-6}$ |
| SUM | / | / | 259.28 mg | $28.212\times10^{-4}$ |

Price of HESE: 1 kg containing 433.384 g $ZnSO_4$, 2.054 g $ZnCl_2$, 3.394 g $ZnBr_2$, 4.819 g $ZnI_2$, and 556.349 g $H_2O$. ~0.334 \$·$kg^{-1}$

And, 2 M ZSO is ~0.317 \$·$kg^{-1}$

## Supplementary References:


1 An, Y. *et al.* Stable Aqueous Anode-Free Zinc Batteries Enabled by Interfacial Engineering. *Advanced Functional Materials* **31**, 2101886, doi:https://doi.org/10.1002/adfm.202101886 (2021).

2 Zhao, K. *et al.* Boosting the Kinetics and Stability of Zn Anodes in Aqueous Electrolytes with Supramolecular Cyclodextrin Additives. *Journal of the American Chemical Society* **144**, 11129-11137, doi:10.1021/jacs.2c00551 (2022).

3 Yin, J. *et al.* Integrated electrolyte regulation strategy: Trace trifunctional tranexamic acid additive for highly reversible Zn metal anode and stable aqueous zinc ion battery. *Energy Storage Materials* **59**, 102800, doi:https://doi.org/10.1016/j.ensm.2023.102800 (2023).

4 Luo, J. *et al.* Regulating the Inner Helmholtz Plane with a High Donor Additive for Efficient Anode Reversibility in Aqueous Zn-Ion Batteries. *Angewandte Chemie International Edition* **62**, e202302302, doi:https://doi.org/10.1002/anie.202302302 (2023).

5 Wang, S. *et al.* Low-Concentration Redox-Electrolytes for High-Rate and Long-Life Zinc Metal Batteries. *Small* **n/a**, 2207664, doi:https://doi.org/10.1002/smll.202207664.

6 Lv, Y. *et al.* Engineering a self-adaptive electric double layer on both electrodes for high-performance zinc metal batteries. *Energy & Environmental Science* **15**, 4748-4760, doi:10.1039/D2EE02687B (2022).

7 Lin, C. *et al.* High-Rate, Large Capacity, and Long Life Dendrite-Free Zn Metal Anode Enabled by Trifunctional Electrolyte Additive with a Wide Temperature Range. *Advanced Science* **9**, 2201433, doi:https://doi.org/10.1002/advs.202201433 (2022).

8 Hu, Z. *et al.* A Self-Regulated Electrostatic Shielding Layer toward Dendrite-Free Zn Batteries. *Advanced Materials* **34**, 2203104, doi:https://doi.org/10.1002/adma.202203104 (2022).

9 Miao, L. *et al.* Aqueous Electrolytes with Hydrophobic Organic Cosolvents for Stabilizing Zinc Metal Anodes. *ACS Nano* **16**, 9667-9678, doi:10.1021/acsnano.2c02996 (2022).

10 Yu, H. *et al.* Reversible adsorption with oriented arrangement of a zwitterionic additive stabilizes electrodes for ultralong-life Zn-ion batteries. *Energy & Environmental Science* **16**, 2684-2695, doi:10.1039/D3EE00982C (2023).

11 Peng, M. *et al.* Polycation-Regulated Electrolyte and Interfacial Electric Fields for Stable Zinc Metal Batteries. *Angewandte Chemie International Edition* **62**, e202302701, doi:https://doi.org/10.1002/anie.202302701 (2023).

12 Li, C. *et al.* Enabling selective zinc-ion intercalation by a eutectic electrolyte for practical anodeless zinc batteries. *Nature Communications* **14**, 3067, doi:10.1038/s41467-023-38460-2 (2023).

13 Li, J. *et al.* Dextran: A Multifunctional and Universal Electrolyte Additive for Aqueous Zn Ion Batteries. *Advanced Energy Materials* **13**, 2301743, doi:https://doi.org/10.1002/aenm.202301743 (2023).

14 Wang, X. *et al.* Highly Reversible Zinc Metal Anodes Enabled by Solvation Structure and Interface Chemistry Modulation. *Advanced Energy Materials* **13**, 2301670, doi:https://doi.org/10.1002/aenm.202301670 (2023).

15 Zhou, K., Li, Z., Qiu, X., Yu, Z. & Wang, Y. Boosting Zn Anode Utilization by Trace Iodine Ions in Organic-Water Hybrid Electrolytes through Formation of Anion-rich Adsorbing Layers. *Angewandte Chemie International Edition* **62**, e202309594, doi:https://doi.org/10.1002/anie.202309594 (2023).

16 Tian, C. *et al.* Improved Interfacial Ion Migration and Deposition through the Chain-Liquid Synergistic Effect by a Carboxylated Hydrogel Electrolyte for Stable Zinc Metal Anodes. *Angewandte Chemie International Edition* **62**, e202310970, doi:https://doi.org/10.1002/anie.202310970 (2023).

17 Li, D., Cao, L., Deng, T., Liu, S. & Wang, C. Design of a Solid Electrolyte Interphase for Aqueous Zn Batteries. *Angewandte Chemie International Edition* **60**, 13035-13041, doi:https://doi.org/10.1002/anie.202103390 (2021).

18 Zhao, R. *et al.* Lanthanum nitrate as aqueous electrolyte additive for favourable zinc metal electrodeposition. *Nature Communications* **13**, 3252, doi:10.1038/s41467-022-30939-8 (2022).

19 Cao, J. *et al.* Interfacial Double-Coordination Effect Guiding Uniform Electrodeposition for Reversible Zinc Metal Anode. *Advanced Energy Materials* **14**, 2302770, doi:https://doi.org/10.1002/aenm.202302770 (2024).

20 Hu, N. *et al.* A Double-Charged Organic Molecule Additive to Customize Electric Double Layer for Super-Stable and Deep-Rechargeable Zn Metal Pouch Batteries. *Advanced Functional Materials* **34**, 2311773, doi:https://doi.org/10.1002/adfm.202311773 (2024).

21 Zhao, Z. *et al.* Horizontally arranged zinc platelet electrodeposits modulated by fluorinated covalent organic framework film for high-rate and durable aqueous zinc ion batteries. *Nature Communications* **12**, 6606, doi:10.1038/s41467-021-26947-9 (2021).

22 Yang, H. *et al.* Sustainable high-energy aqueous zinc–manganese dioxide batteries enabled by stress-governed metal electrodeposition and fast zinc diffusivity. *Energy & Environmental Science* **16**, 2133-2141, doi:10.1039/D2EE03777G (2023).